



UNIVERSITÀ DEGLI STUDI DI PISA
Facoltà di Farmacia

Corso di Laurea Specialistica in
Chimica e Tecnologia Farmaceutiche

Tesi di Laurea:

*Design, synthesis and biological evaluation of heterocyclic
derivatives as potential MAGL inhibitors.*

Relatori:

Prof.ssa Clementina Manera

Dott.ssa Francesca Castelli

Candidato:

Gianfilippo Martello

ANNO ACCADEMICO 2010/2011

A mio cugino Fabio e alla mia famiglia...

Sommario

1. Introduction	5
1.1 Description	5
1.2 Taxonomy	6
1.3 Endocannabinoid system (ECS)	7
1.4 MAGL	9
1.4.1 Structure and most important residues	9
1.4.2 Binding of the natural substrate	13
1.4.3 Catalytic Mechanism	15
1.4.4 MAGL Inhibitors	17
1.4.5 Therapeutic applications of MAGL targeting compounds	29
2. Introduction of Experimental Part	34
2.1 MAGL Inhibitors	35
2.1.1 De novo Inhibitors	36
3. Equipment used in Synthesis	41
4. Scheme of Synthesis	42
4.1 Schema 1	42
4.2 Schema 2	45
4.3 Schema 3	48
4.4 Schema 4	50
5. Experimental Part	53
5.1 2-oxo-1,2-dihydro quinoline-3-carboxaldehyde (1)	53
5.2 1-(4-fluorobenzyl)-2-oxo-1,2-dihydro quinoline-3-carboxaldehyde (2)	54
5.3 1-(4-fluorobenzyl)-3-[(hydroxyimino)methyl]quinolin-2(1H)-one (3)	55
5.4 1-(4-fluorobenzyl)-2-oxo-1,2-dihydroquinoline-3-carbonitrile (4)	56
5.5 3-bromoquinoline 1-oxide (5)	57

5.6	3-bromoquinolin-2(1H)-one (6).....	58
5.7	3-bromo-1-(4-fluorobenzyl)quinolin-2(1H)-one (7)	59
5.8	4-nitrophenyl [1-(4-fluorobenzyl)-2-oxo-1,2-dihydroquinolin-3-yl]carbamate (A2a)	60
5.9	Phenyl [1-(4-fluorobenzyl)-2-oxo-1,2-dihydroquinolin-3-yl]carbamate (A2b)	61
5.10	4-fluorobenzyl 1-(4-fluorobenzyl)-2-oxo-1,2-dihydropyridine-3-carboxylate (8).....	62
5.11	Tert-butyl [1-(4-fluorobenzyl)-2-oxo-1,2-dihydropyridin-3-yl]carbamate (9)	63
5.12	3-amino-1-(4-fluorobenzyl)pyridin-2(1H)-one (10).....	64
5.13	Phenyl [1-(4-fluorobenzyl)-2-oxo-1,2-dihydropyridin-3-yl]carbamate (B1a)	65
5.14	Methyl 1-(4-fluorophenyl)-2-oxo-1,2-dihydropyridine-3-carboxylate (11)	66
5.15	1-(4-fluorophenyl)-2-oxo-1,2-dihydropyridine-3-carboxylic acid (12).....	67
5.16	Tert-butyl [1-(4-fluorophenyl)-2-oxo-1,2-dihydropyridin-3-yl]carbamate (13).....	68
5.17	3-amino-1-(4-fluorophenyl)pyridin-2(1H)-one (14)	69
5.18	Phenyl [1-(4-fluorophenyl)-2-oxo-1,2-dihydropyridin-3-yl]carbamate (B2a)	70
6.	References	71

1. Introduction

1.1 Description

Cannabis is a genus of flowering plant that includes one or more species. The plant is believed to be indigenous to Central Asia, China, and the north-west Himalayas. The common name for Cannabis is hemp, although this term is sometimes used to refer only to strains cultivated for "industrial" (non-drug) use. Cannabis plants produce a unique family of compounds called cannabinoids, several of which produce psychical and/or physiological effects when consumed. The crude drug usually comes in the form of dried flowers and leaves, resin (hashish), or various extracts. The cultivation or possession of Cannabis for drug purposes is outlawed in most countries.



Figure 1

Cannabis is an annual, flowering herb. The leaves are palmately compound, with serrate leaflets. The first pair of leaves usually have a single leaflet, the number gradually increasing up to a maximum of about thirteen leaflets per leaf (usually seven or nine), depending on variety and growing conditions. At the top of a flowering plant, this number again diminishes to a single leaflet per leaf. The lower leaf pairs usually occur in an opposite leaf arrangement and the upper leaf pairs in an alternate arrangement on the main stem of a mature plant.¹



Figure 2 - Leaf of a Cannabis plant

1.2 Taxonomy

The genus Cannabis was formerly placed in the Nettle (Urticaceae) or Mulberry (Moraceae) family, but is now considered along with hops (*Humulus* sp.) to belong to the Hemp family (Cannabaceae). Various types of Cannabis have been described, and classified as species, subspecies, or varieties:

- plants cultivated for fiber and seed production, described as low-intoxicant, non-drug, or fiber types;
- plants cultivated for drug production, described as high-intoxicant or drug types;
- escaped or wild forms of either of the above types.

Cannabis plants produce a unique family of terpeno-phenolic compounds called cannabinoids, which produce the "high" one experiences from smoking marijuana. The two cannabinoids usually produced in greatest abundance are cannabidiol (CBD) and/or Δ^9 -tetrahydrocannabinol (THC), but only THC is psychoactive.

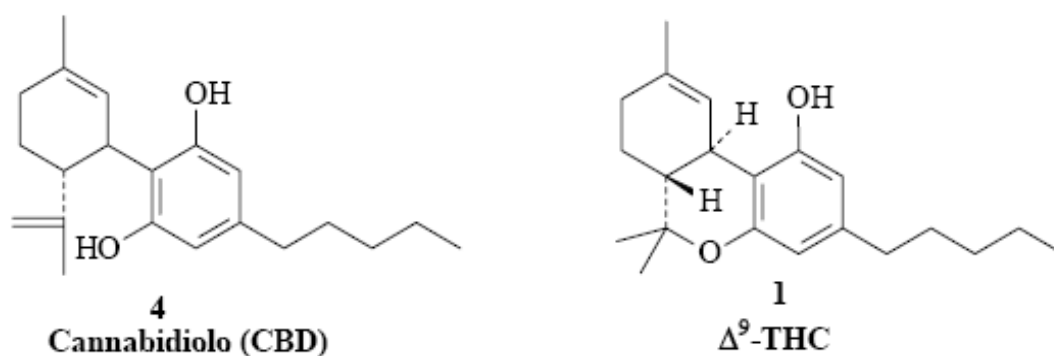


Figure 3

Since the early 1970's, Cannabis plants have been categorized by their chemical phenotype or "chemotype," based on the overall amount of THC produced, and on the ratio of THC to CBD. Although overall cannabinoid production is influenced by environmental factors, the THC/CBD ratio is genetically determined and remains fixed throughout the life of a plant. Non-drug plants produce relatively low levels of THC and high levels of CBD, while drug plants produce high levels of THC and low levels of CBD. When plants of these two chemotypes cross-pollinate, the plants in the first filial (F1) generation have an intermediate chemotype and produce similar amounts of CBD and THC. Female plants of this chemotype may produce enough THC to be utilized for drug production.^{1,2}



Figure 4 - Top of Cannabis plant in vegetative growth stage

1.3 Endocannabinoid system (ECS)

The ECS is constituted by the two cannabinoid receptors (CBRs), the central CB1 and the peripheral CB2 together with their endogenous ligands or endocannabinoids and the enzymes responsible for their metabolism: fatty acid amide hydrolyase (FAAH) and monoglyceride lipase (MAGL). Several molecules have been described to fulfil, at least in some degree, the requirements to be considered endocannabinoids. The proposed endogenous ligands [Figure 5 (1)] are arachidonic acid derivatives in which the acid chain is bound to a polar head group (ethanolamine or glycerol) by amide (such as anandamide or *N*-arachidonylethanolamine (1), AEA), ester (2-arachidonoylglycerol or 2-AG (2) and virodhamine (3)) or ether functionalities (2-arachidylglycerol or noladin ether (4)).

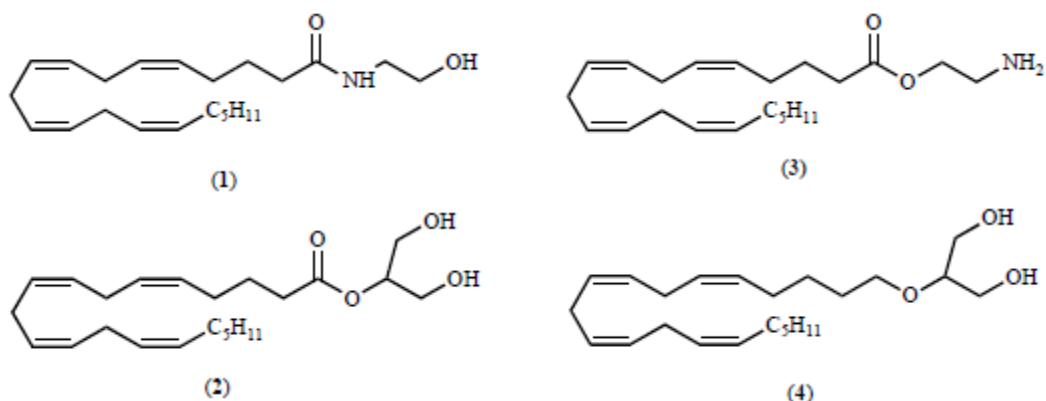


Figure 5 - Structures of the cannabinoid receptor ligands anandamide (1), 2-arachidonylglycerol (2), virodhamine (3) and noladin ether (4)

Among them, AEA and 2-AG are currently considered the primary endocannabinoids, whereas the actual physiological relevance as true endocannabinoids of both virodhamine and noladin ether has been questioned.³

The endogenous ligand of the CB1 receptors is anandamide whereas the endogenous ligand of the CB2 is 2-arachidonylglycerol (2-AG). They are synthesized from membrane-derived phospholipids whose biologic effects are mediated through coupling with the specific, widely expressed ECS receptors located presynaptically. The synthesis of anandamide is Ca²⁺-dependent and is produced locally by the phospholipase D-mediated cleavage of the membrane precursor called N-arachidonoyl-phosphatidylethanolamine (NArPE). While the synthesis of 2-arachidonylglycerol is produced by the diacylglycerols (DAG) lipase cleavage of the membrane precursor. Because endocannabinoids are lipophilic compounds derived from membrane phospholipids, they do not need to be stored in synaptic vesicles like other neurotransmitters. In the brain, they are produced by neurons at their sites of action and act on demand, generating a transient, rapid effect before being hydrolyzed and inactivated by fatty acid amide hydrolase (FAAH), which breaks the amide bond and releases arachidonic acid and ethanolamine. Because of their lipophilic nature and the mechanism of their synthesis and release, endocannabinoids are considered as local neuromodulators.⁴

The ECS has turned out to play key roles in the control of a broad range of physiological functions and, therefore, has become a new exploitable drug target for the treatment of different disorders including neurodegenerative diseases such as multiple sclerosis and Huntington's chorea, excitotoxicity-associated brain damage, and cancer.⁵

However, the therapeutic exploitation of the ECS is not a straightforward and easy strategy. In particular, two main concerns have been raised. The first one is associated with the psychotropic effects associated with CB1 direct activation, and the second one is due to the broad expression of the ECS. Since the ECS is regulating a variety of pathways, any exogenous intervention will potentially alter all of them (although perhaps in different extension) therefore triggering unwanted or unexpected side effects. Both problems can be overcome by taking advantage of the physiologically fine-tuned regulation of the biosynthesis and degradation of the endocannabinoids that avoids both the generation of psychotropic effects as well as general activation of ECS. Based on this premise, a lot of effort has been put in the study of the biosynthetic and degradation pathways of AEA and 2-AG with the objective of developing agents able to induce higher endocannabinoid concentrations in a temporally and spatially controlled manner and relevant only for the desired therapeutic outcome. As such, compounds able to increase the endogenous levels of anandamide have demonstrated therapeutic relevance for the treatment of nociception, inflammation, and neurodegenerative-associated motor symptoms.^{6,7}

1.4 MAGL

1.4.1 Structure and most important residues

MAGL is the metabolic enzyme responsible for the inactivation of 2-AG which is the ligand that interacts predominantly with CB2 receptor.

The first mammalian MAGL molecularly characterized was cloned from a mouse adipocyte cDNA library, therefore, when it was clear that FAAH was not responsible for the inactivation of 2-AG and a 2-AG hydrolyzing activity, distinct from FAAH, was partially purified from porcine brain, MAGL emerged as the most logical candidate. Soon after, a rat brain MAGL was cloned by homology and a MAGL activity described in rat cerebellar membranes.

The primary structure of the proposed rat brain MAGL consists of 303 amino acids, with a molecular weight of 33.4 kDa and a sequence identity of 92% when aligned with the mouse adipocyte MAGL. This high homology has allowed to assign the catalytic triad which has been confirmed by mutagenesis studies in the adipocyte MAGL and it is conserved in the brain MAGL (Figure 6).⁶

The structure of human MAGL was solved at 2.2 Å. resolution by X-ray diffraction. The protein crystallized consist of two molecules per asymmetric unit. The two monomers are in contact by a surface of 884 Å. ; this represents about 7% of the total surface of a monomer. Consistently, MAGL was found as a dimer in a mass spectrometry experiment and no peak corresponding to the monomeric protein was found after gel filtration chromatography. Moreover, both catalytic site entries face the same direction and are thus properly oriented to interact with the membrane in order to recruit the substrates, similar to what was reported following elucidation of the FAAH structure, the main enzyme responsible for anandamide catabolism. Taken together, these data strongly suggest that MAGL is organized as a biological dimer.

According to secondary structure prediction, MAGL architecture presents the hallmark of the α/β hydrolases superfamily. The central β -sheet, constituted of seven parallel and one antiparallel strands, is surrounded by six α helices. A cap domain, which varies much more among the members of this superfamily, covers the structurally conserved β -sheet and the active site. Buried below the cap is the catalytic triad, closely superimposed on that of other hydrolases and haloperoxidases, and made up of residues Ser122, Asp239 and His269. The tridimensional structure thus provides the first direct evidence of the identity of this catalytic triad, previously reported based on mutagenesis studies.

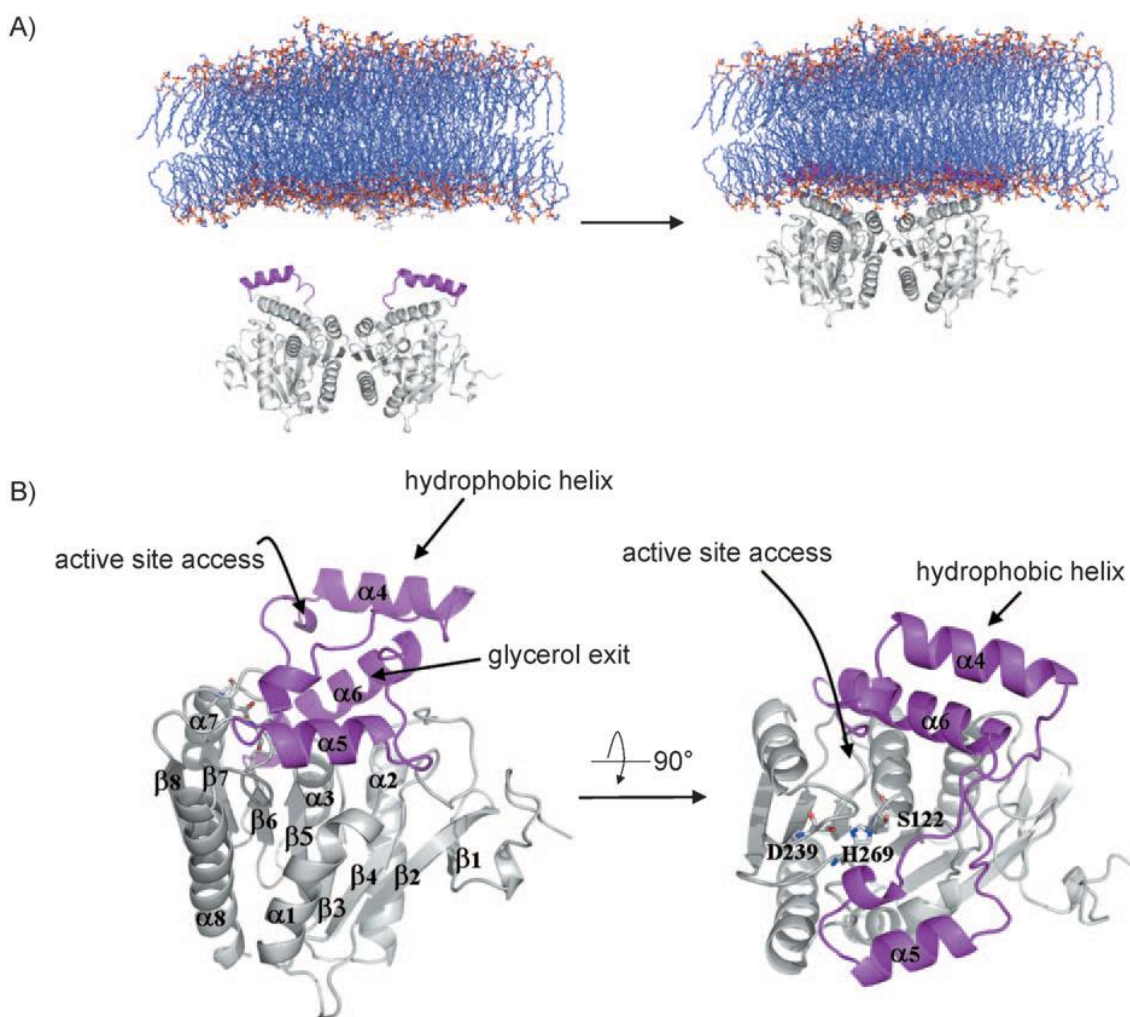


Figure 6 - Overall structure of hMAGL. A) MAGL asymmetric unit. $\alpha 4$ helix is colored magenta. Membrane representation is a palmitoyloleoylphosphatidylethanolamine bilayer minimized using molecular dynamics simulation. B) Left: Side view of a MAGL monomer, with catalytic triad represented as sticks, and cap domain colored magenta. Right: Top view (90° rotation) of the same MAGL subunit.

Four cysteines are present in human MAGL, three of which are located in the vicinity of the catalytic site (Cys201, Cys208, Cys242). Since the first purification of monoacylglycerol lipase, it is known that sulfhydryl-reacting compounds inactivate MAGL. In literature are reported a series of maleimide-based compounds as inhibitors, with Narachidonylmaleimide (NAM) as the most potent representative (Figure 7).

Based on a homology model, it proposed an inhibition mechanism involving a Michael addition of the maleimide moiety on either the Cys208 or Cys242 residue. By mutating rat MAGL residues corresponding to Cys208 and 242, a subsequent study pointed to Cys242 as the crucial residue responsible for this inactivation. The present crystal structure reveals that Cys201 is located near the catalytic site, in a loop connecting $\alpha 5$ to $\alpha 6$ helices (Figure 8).

Accessible from the inside of the catalytic site, Cys201 therefore constitutes a good candidate for the regulation of MAGL activity. On the contrary, Cys208, residing in the $\alpha 6$ helix, points towards the outside of the protein, and hence seems incorrectly placed to react with NAM. To clarify this, it decided to mutate these three cysteines, and to measure the inhibitory potential of NAM.

This study leads to several conclusions. First, when Cys208 is absent, NAM is more available to inhibit MAGL through one or several other cysteine(s). Second, the decrease in NAM inhibitory potency in the C242A mutant reflects the binding of NAM to Cys242, but the weakness of this effect suggests that this event is not a determining factor and only leads to a modest inhibition of activity. Last, the overall increase in pIC50 in the C208A/C242A double mutant is a definite evidence that another cysteine is more crucial than Cys208 or Cys242 for MAGL inhibition by NAM. Indeed, C201A simple mutant showed a substantial decrease in the inhibitory potential. C201A/C208A/C242A triple mutant did not display significant inhibition by NAM.^{8,9}

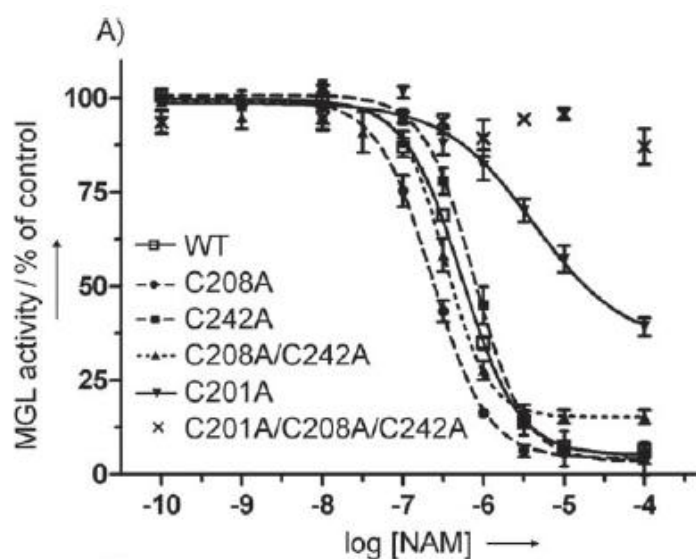


Figure 7 - NAM inhibits human MAGL by targeting Cys201. A) Dose-dependent inhibition of wild-type and mutant MAGL by NAM. Values are expressed as percent of control and represent mean \pm SEM of at least four experiments done in duplicate.

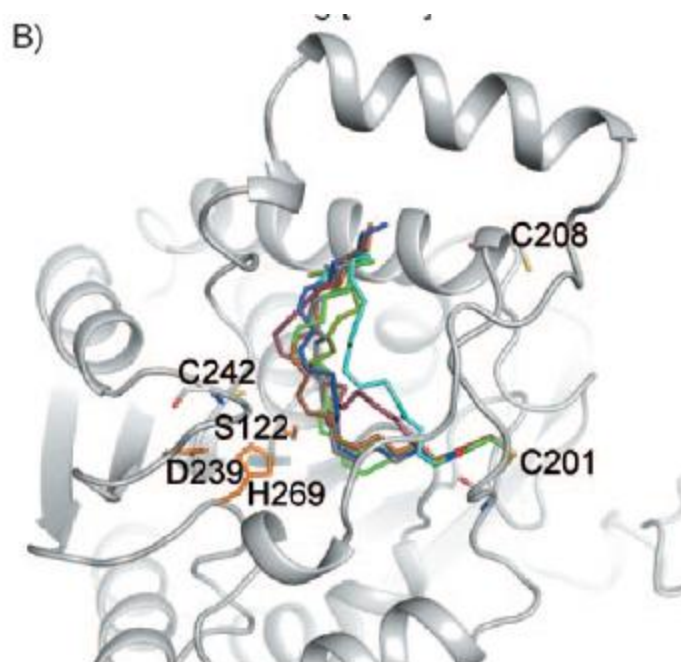


Figure 8 - Docking of NAM in the active site of MAGL, bound to Cys201. The main conformations found by using Gold software are represented with different colours. Catalytic triad is coloured in orange, and Cys201, Cys208 and Cys242 are represented.

1.4.2 Binding of the natural substrate

Elucidation of the MAGL structure provides the first structural basis for rational drug design. To illustrate this and to highlight some key structural features of the active site, 2-AG has been docked in MAGL, simulating the tetrahedral intermediate state covalently bound to Ser122 OG (Figure 9, Figure 10). This reveals a cavity able to accommodate the long and flexible lipid chain of the substrates. This cavity becomes wider as one moves away from the catalytic triad environment, deeply buried in the protein, to the surface of the protein. Several hydrophobic residues cover the channel leading from the surface to the nucleophilic serine. Indeed, Leu148, Ala164, Leu176, Ile179, Leu205, Val207, Ile211, Leu213, Leu214, Val217 and Leu241 side chains are properly located to interact with the arachidonoyl moiety of 2-AG, and mediate the MAGL substrate specificity for lipid substrates.

The near environment of the catalytic triad presents a more hydrophilic character than the channel pointing towards the enzyme surface. Besides the backbone NH from Met123 and Ala51, which form the “oxyanion hole,” the Tyr58 hydroxyl group, the NH from the His121 and His272 side chains, the guanidinium from Arg57, the carboxylate from Glu53, and the backbone carbonyl from Ala51 delimit a polar cavity that accommodates the polar glycerol head group of 2-AG. A glycerol molecule found in this alcohol-binding pocket is in support of the proposed binding mode of 2-AG. A positive electron density feature was apparent in the vicinity of the oxyanion hole at

the end of the structure-refinement process. This was located at the entry of this polar cavity and precisely at the same place as the glycerol moiety in 2-AG docking results.⁹

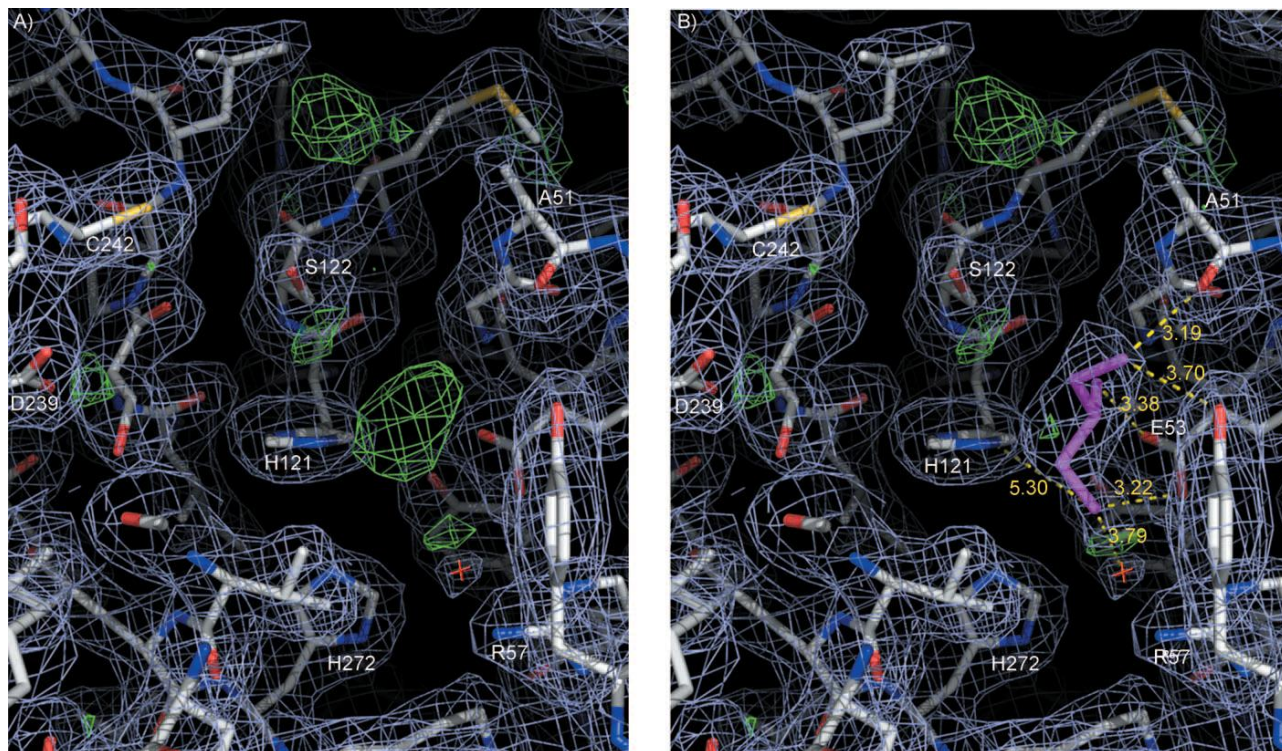


Figure 9

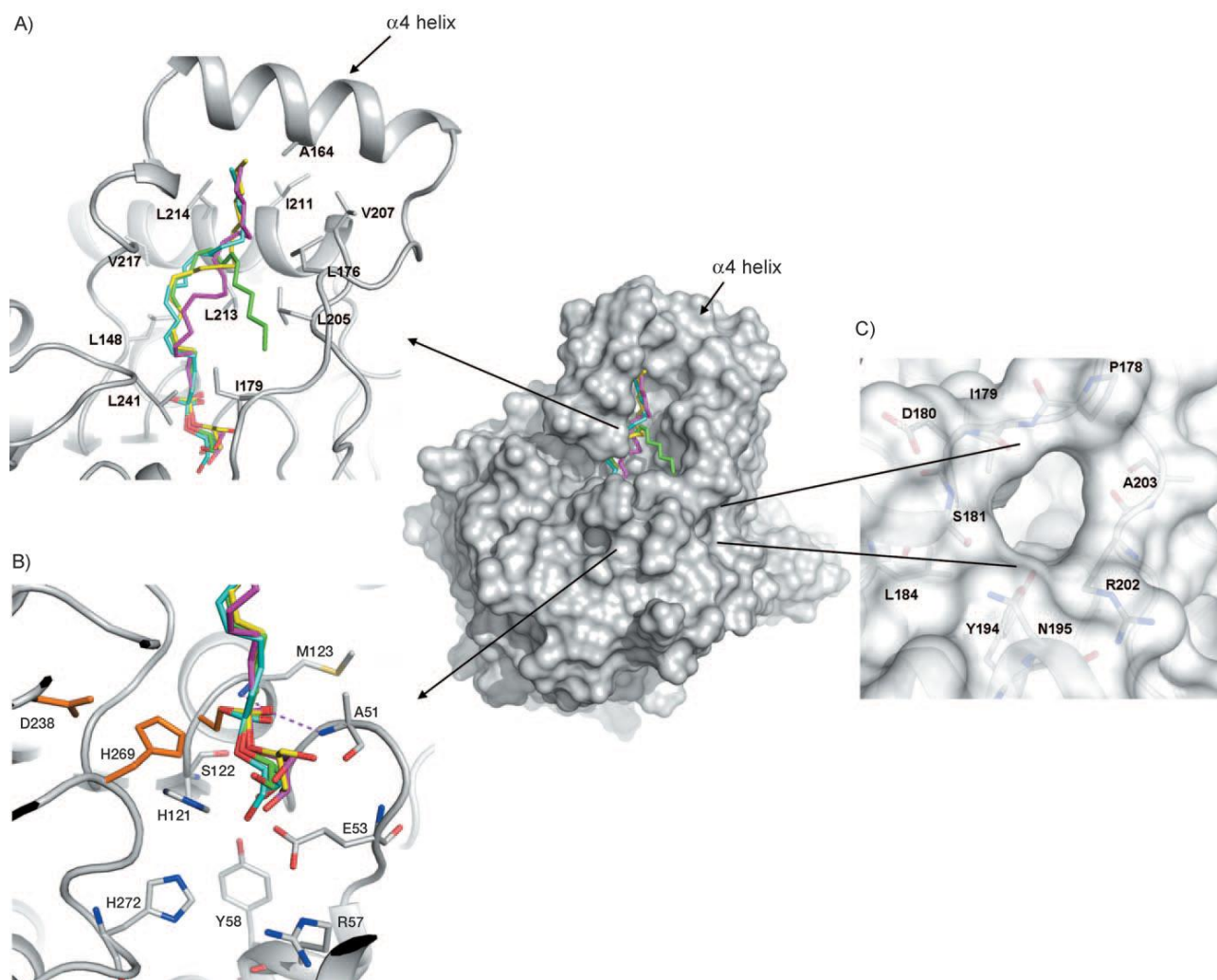


Figure 10 - Docking of 2-AG in the active site of MAGL. The natural substrate is bound in the tetrahedral intermediate state to Ser122. The four first conformations found by using Gold software are represented using different colours. A) Acyl-binding and B) alcohol-binding sites are highlighted, as well as C) the glycerollexit channel. Side chains of residues interacting with the 2-AG acyl moiety or lining the hydrophilic cavity are represented as sticks. The interactions in the oxyanion hole are represented with dashed lines. The $\alpha 4$ helix is also indicated by arrows.

1.4.3 Catalytic Mechanism

The kinetics of lipolytic enzymes can be considered as a two-phase process that includes a first binding step followed by hydrolysis of the substrate. As a general feature of lipases, they can hydrolyse monomeric substrate molecules, but only after binding to the substrate interface, conversion of the aggregated substrate can take place. This initial binding step of the lipase to the lipid-water interface, followed by binding of a single substrate molecule in the active site of the enzyme and catalytic turnover, results in complex kinetics as compared to the situation where both enzyme and substrate are water soluble. Once the substrate reaches the active site, its ester bond is

hydrolysed in a mechanism similar to that of serine proteases. Catalysis is initiated by nucleophilic attack of the serine hydroxyl on the susceptible carbonyl carbon of the substrate. This attack is facilitated by a general acid-base mechanism in which the serine is activated by a hydrogen bond in relay with histidine and aspartate or glutamate. Afterwards, a tetrahedral acyl-enzyme is formed, which is stabilized by the “oxyanion hole”. In general, the “oxyanion hole” is not preformed but is created by the opening of the lid and the exposure of a substrate-binding pocket. Collapse of the tetrahedral adduct in the forward direction involves expulsion of the leaving group (corresponding to the alcohol moiety) and generation of a second acyl-enzyme complex. Finally, the deacylation step involves the attack of a water molecule at the active site. Similarly to the catalytic serine, the water molecule is activated as a more effective nucleophile due to the proton shuttling of the charge-relay system (Figure 11).⁶

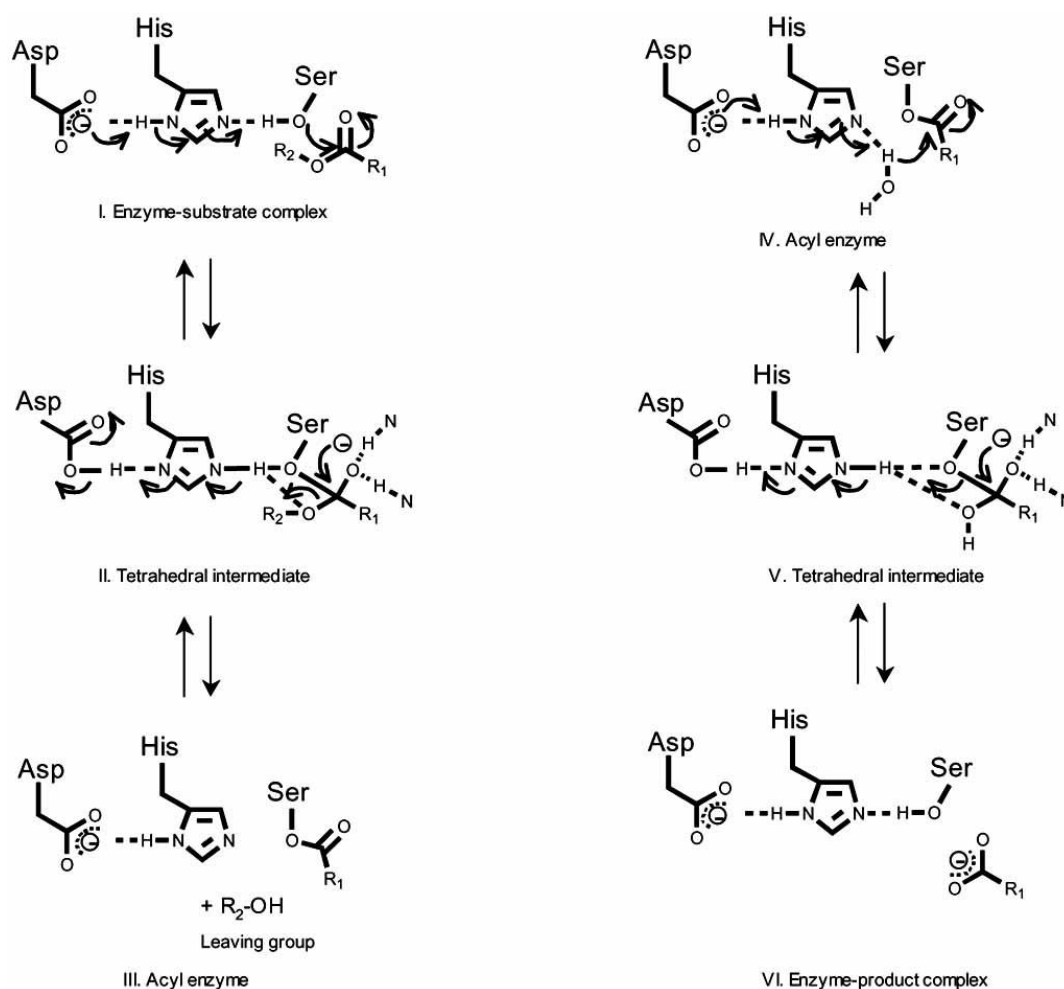


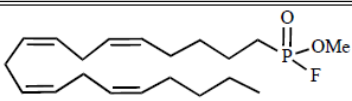
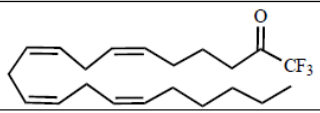
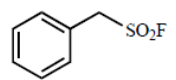
Figure 11 - Schematic representation of the catalytic mechanism based on a catalytic triad of serine (nucleophile), histidine and aspartate. In MAGL the catalytic triad is formed by Ser122, His269 and Asp269.

The close homology between MAGL and the widely studied family of lipases has facilitated the analysis of MAGL structure and its catalytic mechanism. However, MAGL also presents some unique features that clearly differentiate it from other lipases. One of these aspects is its substrate specificity. MAGL hydrolyses 2-monooleoylglycerol at the same rate as 1(3)-monooleoylglycerol with an apparent K_m of 0.2 mM for both substrates at 21 °C and pH 7.4, although it seems to prefer 2-arachidonoylglycerol to its corresponding 1(3)- regioisomer. The optimum pH is 7.0- 8.0. MAGL does not show appreciable activity against diglycerides, triglycerides, cholesterol esters or lysophosphatidylcholine.

1.4.4 MAGL Inhibitors

1.4.4.1 General serine hydrolase inhibitors

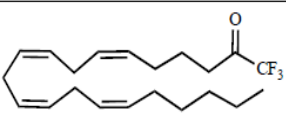
Since mechanistically MAGL is a serine hydrolase, the first wide group of inhibitors are the general serine-hydrolase inhibitors. This series of mechanistically based inhibitors binds in either a reversible or irreversible covalent manner to the nucleophilic serine disrupting its catalytic activity. Chemically, we can distinguish three main reactive groups: fluorophosphonates, trifluoromethylketones and sulfonylfluorides (Table 1, Table 2, Table 3). As the most representative compound within each of these classes we can mention methyl arachidonylfluorophosphonate (MAFP), arachidonyltrifluoromethylketone (ATFMK) and phenylmethylsulfonylfluoride (PMSF). All these compounds are not new to the ECS field, since they are old known FAAH inhibitors. Considering the similarity between the mechanism and the structure of the substrate between MAGL and FAAH, it is clear that one of the first aspects to consider when identifying potential MAGL inhibitors is the selectivity between the two hydrolytic enzymes FAAH and MAGL. In general, these serine hydrolase inhibitors that were previously shown to block FAAH, also inhibit MAGL activity although in a less potent manner (Table 1), with IC_{50} values in the low micromolar range [IC_{50} (MAFP) = $0.8 \pm 0.05 \mu\text{M}$; IC_{50} (ATFMK) = $2.5 \pm 0.04 \mu\text{M}$].

Compound	Structure	IC ₅₀ MAGL (μM)	IC ₅₀ FAAH (μM)
MAFP		0.0022 ± 0.0003 ^a ; 0.8 ± 0.05 ^b ; 0.10 ± 0.02 ^c	0.0025 ^e
ATFMK		2.5 ± 0.04 ^b ; 66 ± 9 ^d	1.9 ^e
HDSF	CH ₃ -(CH ₂) ₁₅ -SO ₂ F	0.241 ± 0.017 ^a ; 6.2 ± 0.1 ^b	0.0102 ^f
PMSF		155 ± 7 ^a	0.9 ^e

Values from references ^a[43], ^b[74], ^c[77], ^d[118], and ^e[34]. ^f75% inhibition at 1 mM, reference [75].

Table 1 - Inhibition of 2-AG and AEA Hydrolysis by General Serine Hydrolase Inhibitors

Even hexadecylsulfonylfluoride (HDSF, also referred as AM374), a potent inhibitor of FAAH (IC₅₀ = 10.2 ± 0.1 nM), showed a significant inhibiting activity towards MAGL (IC₅₀ = 6.2 ± 0.1 μM). A parallel behaviour for these compounds has been recently described by the group of Saario, reporting IC₅₀ values for MAGL inhibition of 241 nM for HDSF, 155 μM for PMSF and 2.2 nM for MAFP. Discrepancies in IC₅₀ values probably reflect differences in the source of enzyme (MAGL overexpressed in HeLa cells or rat cerebellar membranes) as well as other variations in experimental protocols. Extending this mechanistic approach but trying to gain some selectivity towards MAGL versus other serine hydrolases, especially FAAH, a series of compounds with modifications in the side chain that bears the reactive group has been developed (Table 2). In this regard, arachidonyl-, oleyl- and palmityltrifluoromethylketones have been studied [IC₅₀ (MAGL) = 2.9, 1.0, and 7.8 μM, respectively], but they are still more potent inhibitors of FAAH (IC₅₀ = 0.55, 0.076, and 0.073 μM, respectively).

Compound	Structure	IC ₅₀ MAGL (μM)	IC ₅₀ FAAH ^f (μM)
ATFMK		66 ^a 2.5 ± 0.04 ^b 2.9 ^c	0.55
OTMK	CH ₃ (CH ₂) ₇ CH=CH(CH ₂) ₇ COCF ₃	1.0 ^c	0.076
PTMK	CH ₃ (CH ₂) ₁₄ COCF ₃	7.8 ^c	0.073

Values from references ^a[43], ^b[74] and ^c[75].

Table 2 - Inhibition of 2-AG and AEA Hydrolysis by Trifluoromethylketones

Further modification of the trifluoromethylketone moiety with the introduction of a sulfide (R-S-) group in the α position, structural motif known to inhibit esterases, has been also analysed in a brief SAR study aimed at the search of new antitumor agents acting as MAGL inhibitors (Fig. 12). From the experimental values of this series of compounds, it is observed that the inhibition of degradation of 2-AG and 2-OG is increased with the length of the alkyl chain (R). The percentage values of hydrolysis of 2-OG as compared with control are 92.4, 71.8, 67.7, and 56.3% for hexyl-, octyl-, decyl-, and dodecylthiotrifluoropropanones.

Bulky groups [R = Ph-(CH₂)₂-] attached to sulfur leads to a decay of the inhibitory effect and other structural variations such as oxidation of sulfide to sulfone, replacement of the trifluoromethylketone moiety (-CF₃) by methylketones (-CH₃), and the substitution of the sulfur for an oxygen atom result in a loss of the inhibition properties.

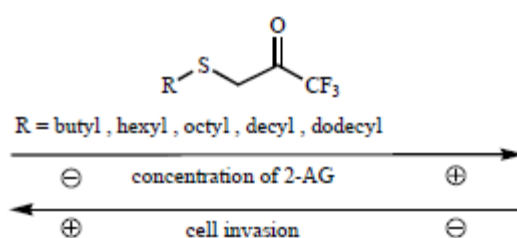
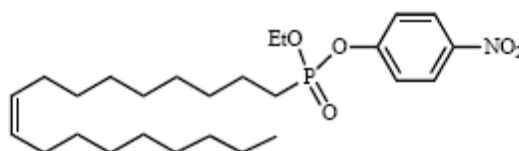


Figure 12 - Effect of the introduction of a α -sulfide group (R-S-) in trifluoromethylketones on 2-AG hydrolysis and invasion of prostate cancer cells.

However, neither IC₅₀ values nor data about the selectivity of these compounds are reported.

Replacing the trifluoromethylketone with a different reactive moiety produced a series of phosphonate esters of oleic acid that has been recently screened for its ability to inhibit MAGL. Nevertheless, none of the analysed compounds exerted a remarkable inhibition towards MAGL, UP101 (Table 3) being the most potent compound with only a moderate IC₅₀ value (IC₅₀ = 3.2 μ M) and largely nonselective behaviour upon the rest of targets studied, including FAAH, *sn*-1 diacylglycerol lipase α and CB1 and CB2 cannabinoid receptors.⁶



Target	IC ₅₀ (μM) ^a
MAGL (COS cell cytosol)	3.2 ± 0.17
DAGLα (human recombinant)	3.7 ± 0.2
FAAH (rat brain membranes)	0.18 ± 0.14
CB ₁ (human recombinant)	5 ± 0.2
CB ₂ (human recombinant)	10 ± 0.14

^aData from reference [77].

Table 3 - Structure and Inhibition Profile of UP101

1.4.4.2 Inhibitors inspired by the endogenous substrate: 2-AG analogues

With the aim of searching for selective inhibitors of MAGL, a logical starting point is to use the known endogenous substrate as initial template and make structural variations looking for the optimal potency, selectivity, and metabolic stability. In the structure of 2-AG we can distinguish three main parts susceptible to modifications: i) fatty acid chain, ii) linker and iii) glycerol moiety (Figure 13). Based on this, the abilities of a series of analogues of 2-AG have been examined (Table 4) in their ability to inhibit cytosolic MAGL activity. With respect to the fatty acid chain, the experimental data reveal that both isomers 2-AG and 1-AG are equipotent in disrupting MAGL activity (IC₅₀ = 13 and 17 μM, respectively).

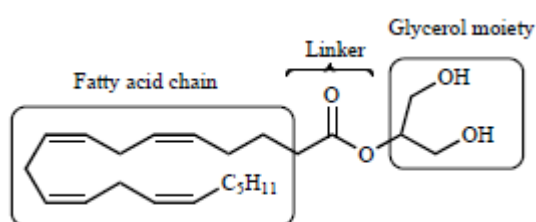


Figure 13 - 2-AG structure: points of structural modification

Shorter homologues, such as 2-OG and 2-linoleoylglycerol (2-LG), retain the values of affinity for MAGL but show diminished selectivity towards FAAH. Branching and introduction of a hydroxyl group at the end of the chain, as in O2204, maintains the affinity towards MAGL (IC₅₀ = 14 μM) while gaining a slight affinity towards FAAH (IC₅₀ = 35 μM).

In the linker moiety, replacement of the ester group of 2-AG by an amide linkage in arachidonoylserinol ($IC_{50} = 73 \mu M$) or an ether in noladin ether ($IC_{50} = 36 \mu M$) leads to weaker inhibitors of MAGL, while introduction of the urea moiety (O1502) produces an almost complete loss of inhibition of MAGL (only 39% inhibition at $100 \mu M$). Finally, the effect of modifications in the glycerol part was also examined. Thus, substitution of the glyceryl moiety by a thienylmethyl group as in CAY10402 abolishes MAGL activity while keeping a low FAAH inhibitory potency ($IC_{50} = 10 \mu M$). Within this category fall 2-OG and 2-linoleoylglycerol (2-LG), retain the values of

affinity for MAGL but show diminished selectivity towards FAAH. Branching and introduction of a hydroxyl group at the end of the chain, as in O2204, maintains the affinity towards MAGL ($IC_{50} = 14 \mu M$) while gaining a slight affinity towards FAAH ($IC_{50} = 35 \mu M$). In the linker moiety, replacement of the ester group of 2-AG by an amide linkage in arachidonoylserinol ($IC_{50} = 73 \mu M$) or an ether in noladin ether ($IC_{50} = 36 \mu M$) leads to weaker inhibitors of MAGL, while introduction of the urea moiety (O1502) produces an almost complete loss of inhibition of MAGL (only 39% inhibition at $100 \mu M$). Finally, the effect of modifications in the glycerol part was also examined. Thus, substitution of the glyceryl moiety by a thienylmethyl group as in CAY10402 abolishes MAGL activity while keeping a low FAAH inhibitory potency ($IC_{50} = 10 \mu M$). Within this category fall a couple of old known compounds, N-(4-hydroxy-2-methylphenyl) arachidonamide (VDM11) and N-4-(hydroxyphenyl) arachidonamide (AM404). Originally proposed as anandamide uptake inhibitors, they are also FAAH inhibitors. Therefore, they were also tested as MAGL inhibitors. This work reveals that AM404 and its analogue VDM11 inhibited the metabolism of anandamide by rat brain FAAH equipotently ($IC_{50} = 2.1$ and $2.6 \mu M$, respectively) and to a lesser extent the degradation of 2-OG by cytosolic MAGL ($IC_{50} = 21$ and $20 \mu M$, respectively). In addition, the study showed that there are discrepancies in the inhibitory potency of FAAH and MAGL due to experimental conditions. Thus, the absence of fatty-acid free bovine serum albumin (BSA) produces a higher sensitivity of FAAH towards VDM11 ($IC_{50} = 1.6 \mu M$). A similar effect of BSA was observed for the inhibitory capacity of VDM11 towards membrane bound MAGL (IC_{50} from $14 \mu M$ to $6 \mu M$) and other arachidonoyl-based compounds such as arachidonoylserinol (IC_{50} from $24 \mu M$ to $13 \mu M$). These studies suggest that the presence of BSA could alter the real concentration of these lipophilic (and sticky) substrates and inhibitors and therefore, be the origin of the discrepancies found between different reported values. For compounds see Table 4.⁶

Compound	Structure	IC ₅₀ (μM) MAGL ^a	IC ₅₀ (μM) FAAH ^a
2-AG		13	37% ^b
1-AG		17	42% ^b
2-OG	$\text{CH}_3(\text{CH}_2)_7\text{CH}=\text{CH}(\text{CH}_2)_7$	15	2.5
2-LG	$\text{CH}=\text{CH}(\text{CH}_2)_7$ $\text{CH}=\text{CH}(\text{CH}_2)_4\text{CH}_3$	12	22
O2204		14 ^c	35
Arachidonoylserinol		73	78
Noladin ether		36	3
O1502		39% ^b	19
CAY10402		14% ^b	10
VDM11		20	2.6
AM404		21	2.1

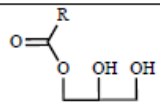
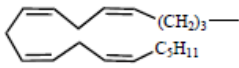
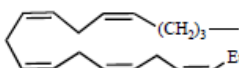

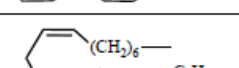
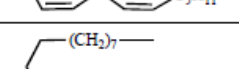
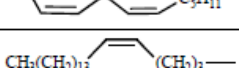
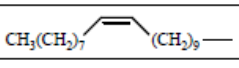
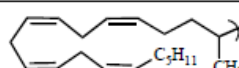
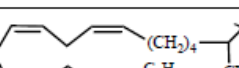
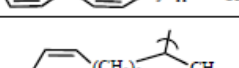
^aData from references [75] and [79]. ^bPercentage of inhibition at 100 nM. ^cSince this compound did not produce complete inhibition, the reported IC₅₀ value was calculated from the inhibitable component (75 ± 6%) [75].

Table 4 - Inhibition of MAGL and FAAH by 2-AG Analogues

1.4.4.3 Inhibitors inspired by the endogenous substrate: 1-AG Homologues

Since 1-AG shows comparable potency to 2-AG as MAGL inhibitor (IC₅₀ (1-AG) = 17 μM and IC₅₀ (2-AG) = 13 μM, Table 4) but it is more stable in biological solutions, a group of analogues of 1-AG have been examined as MAGL inhibitors. The structural study (Table 5) includes variations in length (14-22 carbons) and number of unsaturations (0-5) of the fatty acid chains. The main

conclusions of this study indicate that for cytosolic MAGL the number of unsaturations does not affect significantly the interaction as the IC₅₀ values range between 4.5 and 21 μM. However, a decay of inhibition is observed for the monounsaturated compounds (O3908 and O4066) and a total loss of activity for the saturated C-20, 1-arachidinoylethanolamide. In contrast, shorter fully saturated compounds such as 1-palmitoylethanolamide (C-16) and 1-myristoylethanolamide (C-14) inhibit MAGL (IC₅₀ values of 12 and 32 μM, respectively). The lack of effect of the C-20 analogue has been attributed by the authors to its lower solubility that prevents to reach the threshold critical concentration needed to interact with the enzyme. The introduction of a methyl group in the α position to the acyl group does not produce a clear tendency in the inhibitory capacity in comparison with the analogues lacking the methyl group (1-AG vs. O1428, O3872 vs. O4081, and O3846 vs. O3973). Regarding selectivity, most of the compounds in this series inhibit FAAH activity with similar values (IC₅₀ = 5.7-23 μM) and as previously observed for MAGL, the fully saturated 1-arachidinoylethanolamide does not inhibit the activity of FAAH.

			
Compd	R	IC ₅₀ (μM) MAGL ^a	IC ₅₀ (μM) FAAH ^a
1-AG		7.1; 17 ^b	6.2; 42% ^{b,c}
O3832		8.2	7.6
O3872		4.5	14
O3846		7.5	23
O3907		5.1	5.7
O3908		21	11
O4066		19	10
1-arachidinylglycerol	CH ₃ -(CH ₂) ₁₈ -	19±% ^c	10±3% ^c
1-palmitoylglycerol	CH ₃ -(CH ₂) ₁₄ -	12	8.0
1-myristoylglycerol	CH ₃ -(CH ₂) ₁₂ -	32	18
O1428		15	28±3% ^b
O4081		5.8	5.1
O3973		4.2	2.4

Data from reference ^a[80] and ^b[75]. ^cPercentage of inhibition at 100 μM.

Table 5 - Inhibition of MAGL and FAAH by a Series of 1-AG Analogues

In a further attempt to improve the pharmacological profiles of the compounds, additional structural modifications on the fatty acid chain have been examined by the group of Fowler, although with overall low success in increasing the inhibitory capacities of the compounds. In this series of inhibitors, the arachidonoyl side chain of 1-AG has been replaced by cyclooxygenated chains related to prostaglandins (PG), including PGD₂-1G, PGE₂-1G and PGF₂α-1G (Fig. 6). However, these compounds showed a very weak effect upon MAGL, inhibiting only about 24-37% of MAGL activity at 100 μM of a compound. Similarly, the cyclooxygenated analogues of arachidonoylserinol (PGD₂-serinolamide), AEA (PGD₂-ethanolamide) and arachidonic acid (PGD₂) lack any significant effect on MAGL activity. For compound see Table 5.⁶

1.4.4.4 De novo inhibitors

Two inhibitors of MAGL have been recently described whose structures (Table 6) do not resemble any endogenous cannabinoid. URB754 was reported to inhibit 2-AG degradation through a non competitive and irreversible mechanism with an IC_{50} value of 200 nM measured in rat brain MAGL expressed in HeLa cells. Besides, it showed a high degree of selectivity towards FAAH of about 150 fold ($IC_{50} = 31.8 \mu M$). The other MAGL inhibitor identified, URB602, showed a lower capacity to disrupt MAGL hydrolysing activity (IC_{50} 28-75 μM depending on the source of enzyme) but did not affect the FAAH catalytic activity.⁶

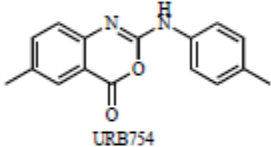
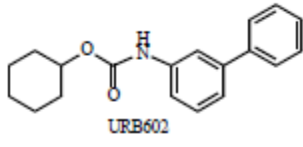
Compound	IC_{50} MAGL ^a	IC_{50} FAAH ^b
 URB754	200 ± 16 nM	31.8 ± 3.8 μM
 URB602	75 ± 7 μM 28 ± 4 μM ^c	No inhibition

Table 6 - Inhibitory Potencies of URB754 and URB602 Towards MAGL and FAAH

Another inhibitor of this class of compounds is SAR629, a derivative of the triazolo-carboxamide series. It shows a nanomolar activity range that is in keeping with that of other carbamate-containing compounds its mechanism of inhibition mimics the pathway of 2-AG hydrolysis by MAGL by making a relatively stable carbamate adduct with the catalytic serine instead of the relatively labile ester adduct.

In the analysis of model in which SAR629 and MAGL bound covalently, the compound adopts a Y shape with its two fluorophenyl moieties pointing toward opposite directions and perpendicular to each other. These moieties are perpendicular to the piperidine linker that adopts a chair conformation. In addition to the covalent bond with Ser122, SAR629 interacts with MAGL essentially by hydrophobic interactions and few polar interactions. Water-mediated interactions occur between the inhibitor nitrogen piperazine or oxygen atoms of its carbamate function and His269 side-chain or Ala61 main-chain carbonyl oxygen (Figure 14).

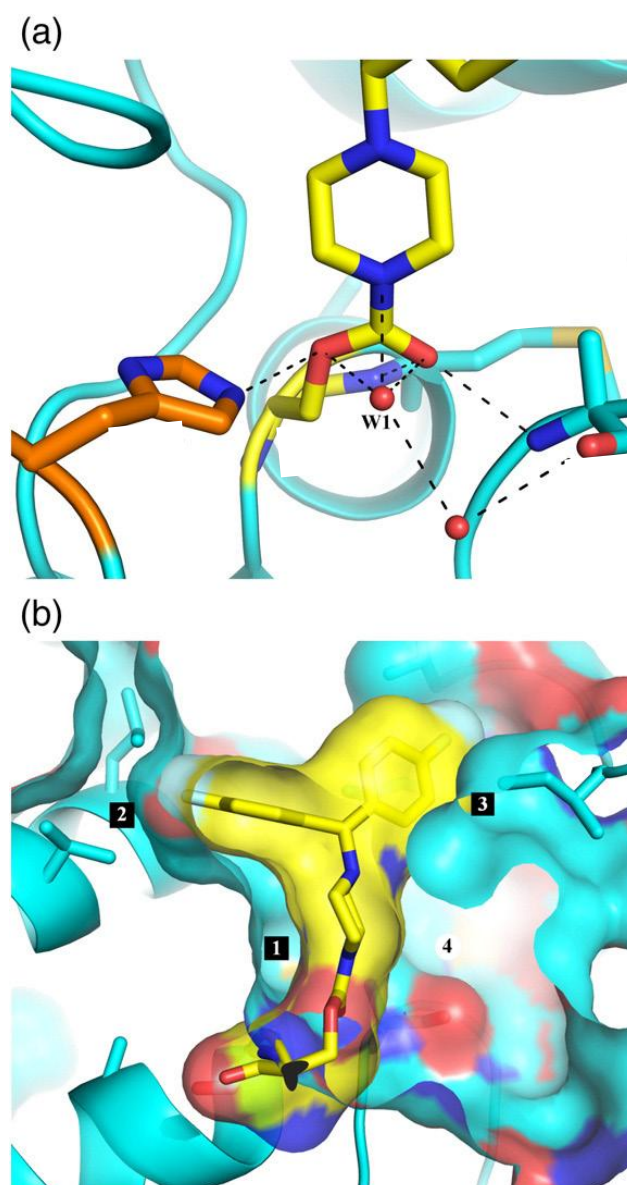


Figure 14

The piperazine moiety is in contact with the protein only via van der Waals interactions on one side (Figure 14b, square 1), but makes no contact on the other side. The nitrogen atoms of the piperazine are not involved in any polar contacts with the protein. One of the fluorophenyl moieties of SAR629 fits in a pocket consisting of Leu158, Leu223, and Leu224, creating van der Waals interactions (Figure 14, square 2). The other fluorophenyl ring is sandwiched between Leu186, Ile189, and Leu215 side chains (Figure 14b, square 3) and points toward a pocket rich in polar atoms (namely, main-chain carbonyl oxygen atoms of Leu186, Gly187, and Pro188 and main chain nitrogen of Ile189). The only direct polar contact between protein and inhibitor occurs between main-chain nitrogen atoms of Ala61 and Met133 (oxyanion hole) and the carbonyl oxygen of SAR629 (Figure 14). The covalent bond formation between Ser122 and the carbon of the

carbamate function is thought not to be fully irreversible. It is supposed that a water molecule is able to hydrolyze the carbamate function connecting the catalytic serine and the inhibitor; however, this process is supposed to be slow.

According to this knowledge is possible to affirm that the carbonyl oxygen of the urea function seems necessary to create the only polar interaction between the inhibitor and the protein. One of the fluorophenyl groups is positioned just above a “plateau” of hydrophobic residues. The role of the piperazine is to orient the other moieties toward pharmacophoric points, and it could probably be replaced by other moieties. The reported MAGL inhibitor JZL184 has a chemical structure very close to that of SAR629 (Figure 15c). Its mechanism of inhibition and its mode of recognition should be similar. Indeed, a carbamate adduct on the catalytic serine has been detected by liquid chromatography–tandem mass spectrometry experiments. Another pocket can also be used as anchoring point in the design of new potent inhibitors. It is filled by one of the fluorophenyl moieties of SAR629 with the fluoride pointing toward a polar region that could be exploited.^{10, 11, 12}

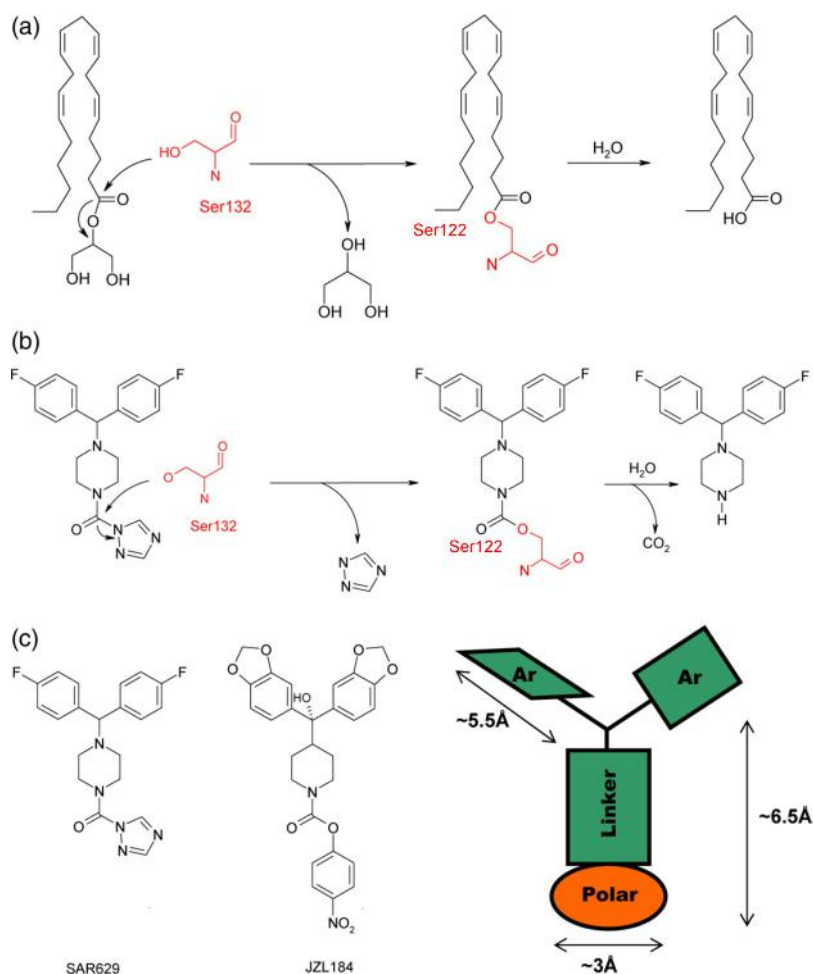
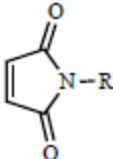
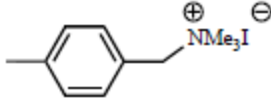
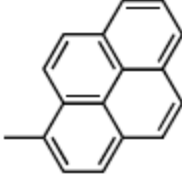
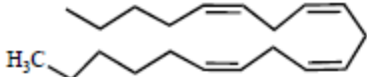
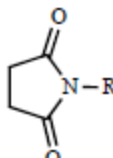
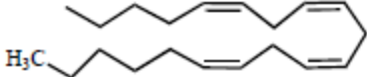


Figure 15 - Reaction mechanism between catalytic Ser122 and 2-AG (a) or SAR629 (b). Pharmacophoric mapping of SAR629 is shown in (c). Dark green elements depict flat and hydrophobic pharmacophoric points, whereas the orange element depicts a polar pharmacophore. Ar, aromatic

1.4.4.5 Inhibitors targeting the essential sulfhydryl group of MAGL

The presence of some thiol groups close to the catalytic site of the enzyme led to the design of NEM analogues as MAGL inhibitors (Table 7). Maleimide analogues behave as Michael acceptors toward thiol residues, binding irreversible to the enzyme.⁶

	
R	IC ₅₀ (μM) ^a
H	70 ± 6
Et	53 ± 7
Pr	53 ± 6
c-Hex	51 ± 6
Ph	44 ± 6
OH	413 ± 23
	68 ± 7
	9.2 ± 0.8
	0.140 ± 0.005
	
R	IC ₅₀ (μM) ^a
H	b
	c

^aData from reference [71]. No inhibition at ^b10 mM or ^c1 mM.

Table 7 - Inhibition of MAGL by Maleimide and Succinimide Derivatives in Rat Cerebellar Membranes

1.4.5 Therapeutic applications of MAGL targeting compounds

In the last years, several studies have demonstrated the key physiological roles of 2-AG. Accordingly, the design and synthesis of compounds able to inhibit MAGL could offer new

perspectives in the understanding and treatment of several disorders. Some of the most promising applications are discussed below.⁶

Neuroprotection and Neurodegenerative Diseases: different studies suggest that endocannabinoids are neuroprotective in different *in vivo* and *in vitro* models. They can protect neurons from hypoxic injury and may represent endogenous neuroprotective molecules in cerebral ischemia. For example, 2-AG protects rat cerebral neurons from ischemia *in vitro* and increases cell viability when these cells are subjected to hypoxia and glucose deprivation. Additionally, levels of endogenous 2-AG were found significantly elevated in the closed head injury model in mice and 2-AG administration produced significant reduction of brain oedema and infarct volume, better clinical recovery, and reduced hippocampal cell death. The protection induced by 2-AG has been attributed to CB1 activation, since this effect was attenuated by the CB1 selective antagonist SR141716A and was absent in CB1(-/-) mice. This mechanism could involve inhibition of intracellular inflammatory signaling pathways, considering that 2-AG abolished the three- to four-fold increase of the expression of the nuclear factor α B (NF- α B). Furthermore, the relation between 2-AG and epilepsy has also received attention. Since cannabimimetic molecules including Δ 9-(-)-tetrahydrocannabinol (Δ 9-THC) are known to depress neurotransmission and to exert anticonvulsant activities, endogenous 2-AG produced during neural excitation could play a regulatory role in calming the enhanced synaptic transmission. In this regard, 2-AG inhibits the depolarization-induced increase in intracellular calcium in NG108-15 cells, thereby modulating several neural functions in this cell type. Hence, 2-AG could prevent the excessive excitability that takes place in epilepsy. Another interesting aspect is the possible implication of 2-AG in neurodegenerative diseases, such as multiple sclerosis (MS). For instance, in areas associated with nerve damage in the MS model of chronic relapsing experimental autoimmune encephalomyelitis (CREAE), increased levels of AEA and 2-AG were detected, suggesting a protective role of these endocannabinoids. In a different animal model of MS, experimental autoimmune encephalomyelitis (EAE), AEA and 2-AG levels were found to be decreased in brain motor related regions (striatum, midbrain). Recently Witting *et al.* showed that in EAE the protective role of endocannabinoids can be disrupted by the action of interferon- α (IFN- α). The massive release of IFN- α by the primed T cells invading the CNS blocks the activation of purinergic P2X7 receptors, the key step that induces 2-AG production by microglia. The disruption of the endocannabinoid-mediated neuroprotection induced by IFN- α occurs without affecting the functionality of the

cannabinoid receptors, thus providing additional support for the use of an endocannabinoid-based medicine to treat MS.⁶

Feeding Behaviour: Marijuana and its major psychotropic component, Δ^9 -THC, were found to stimulate appetite and increase body weight in wasting syndromes. Additionally, endocannabinoids have been involved in the control of energy balance and food intake and their effects have been described as mainly CB1-mediated, since they are antagonized by SR141716A. They may also stimulate lipogenesis and fat accumulation. Therefore, endocannabinoids add to the list of the numerous neurotransmitters and neuropeptides involved in the physiological control of appetite and satiety. In particular, 2-AG has been described to stimulate feeding in a potent and dose-dependent manner, effect blocked in part by the action of SR141716A. Interestingly, the neurohormone leptin, which is the main regulator of the hypothalamic orexigenic and anorectic signals, exerts a negative control on the AEA and 2-AG levels. Considering the role played by endocannabinoids in the intricate network that regulates feed control, the manipulation of their levels could offer useful approaches to the treatment of eating disorders as well as metabolic syndromes.⁶

Cancer: The endocannabinoid system is implicated in cancer because it plays a fundamental role in the control of the cell survival/death decision. Although both endocannabinoids, AEA and 2-AG, have been found to inhibit proliferation of certain cancer cell lines, we will focus on the effects of the latter. 2-AG inhibits proliferation of human breast (EFM-19) and prostate (DU-145) cancer cell lines. 2-AG has been also involved in cancer cell invasion. Block of 2-AG metabolism increases endogenous 2-AG levels, which inhibits invasion of the androgen-independent prostate cancer cells PC-3 and DU-145. These effects have been linked to CB1 receptor activation, considering that CB1 is expressed in these prostate cancer cell lines as well as in the human prostate gland (at a level comparable with the CB1 expression in cerebellum) where it negatively regulates adenylyl cyclase activity. Because prostate cancer has become the most common cancer in men, identifying novel targets and new agents for its treatment has become an imperative issue. Supporting a more general role of 2-AG in tumoral processes, the 2-AG-mediated inhibition of cell proliferation can take place in other types of cancer cell lines such as colorectal carcinomas and C6 glioma cells. Also, tumors such as meningiomas show a massive enhancement in the levels of 2-monoacylglycerols including 2-AG. Therefore, it has been suggested that endocannabinoids could act as endogenous anti-tumour mediators by stimulation of both cannabinoid and non-

cannabinoid receptor mediated mechanisms. Considered together, all the above data have raised the view that the design and synthesis of new compounds that block 2-AG degradation may open new possibilities in the treatment of these types of cancer.^{6, 13}

Drug Dependence: The brain reward system constitutes another point of interest for 2-AG since it has demonstrated a remarkable capacity to attenuate the naloxone-precipitated withdrawal signs in morphine-dependent mice. This result is in agreement with the proposed upregulation of cannabinoid CB1 receptors in morphine dependence, and it supports the hypothesis that either accelerators of endocannabinoid synthesis or inhibitors of its degradation may have a therapeutic potential to treat opiate withdrawal symptoms. The profound changes that the ECS undergoes during the different phases of sensitization to morphine in rats provide a possible neurochemical basis for this cross-sensitization between opiates and cannabinoids. Moreover, 2-AG could play a role in alcohol addiction and in addictions to other drugs such as marijuana, nicotine, and cocaine by activation of the same or related reward pathways.⁶

Other Disorders: It is known that endocannabinoids induce analgesia. For example, when the MAGL inhibitor URB602 is microinjected into the periaqueductal grey matter, it induces in a CB1-dependent manner an increase in the levels of 2-AG, which has been related to an enhancement of the stress-induced analgesia. These effects, which run parallel to those observed after inactivation of anandamide degradation, suggest that 2-AG as well as anandamide could mediate opioid-independent stress-induced analgesia. Another aspect of interest is the presence of the CB1 receptor and both AEA and 2-AG in ocular tissues. Cannabinoids have shown capacity to reduce the ocular hypertension and, in particular, topical application of anandamide was shown to decrease the intraocular pressure in normotensive rabbits. Moreover, topical administration of 2-AG and noladin ether also decreased intraocular pressure in rabbits, reduction that has been attributed to the CB1 receptor. These effects could be of direct application in glaucoma, the disorder characterized by a pathological enhancement of the intraocular pressure. In this regard, the levels of 2-AG and *N*-palmitoylethanolamine have been found to be significantly decreased in the ciliary body in eyes from patients with glaucoma, further supporting the role of these endogenous compounds in the regulation of intraocular pressure.

Finally, the role of 2-AG in the immune system and in particular its effect on the motility of human natural killer cells should be noted, 2-AG induces the migration of KHYG-1 cells (a natural killer

leukemia cell line) and human peripheral blood natural killer cells. This migration can be blocked by the presence of the CB2 antagonist SR144528, and interestingly, it does not occur in the case of AEA or Δ^9 -THC. Accordingly, it has been suggested that 2-AG could contribute to the host-defense mechanism against infectious viruses and tumor cells.⁶

2. Introduction of Experimental Part

Monoacylglycerol lipase (MAGL) is a metabolizing enzyme which belongs to the endocannabinoid system. The endocannabinoid system includes the endogenous ligands: anandamide (AEA) and 2-arachidonoyl glycerol (2-AG) (Figure 16), the cannabinoid receptors CB1 and CB2, the anandamide transporter protein, and two metabolizing enzymes: fatty acid amide hydrolase (FAAH) which is involved in the inactivation of AEA and monoglyceride lipase (MAGL or MGL) which is involved in the inactivation of 2-AG.³

2-AG is the natural ligand for CB1 and CB2 receptors even if it interacts predominantly with CB2 receptors, it exhibits lower affinity than AEA and it is considered the primary endogenous cannabinoid in the brain.

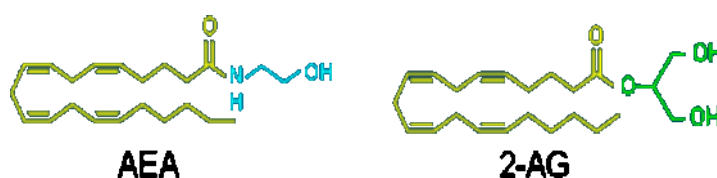


Figure 16

Biological activities of 2-AG have been reported in: immune function, cell proliferation, embryo development, neuroprotection, immunomodulation, cardiovascular function and inflammatory responses.

MAGL is a serine hydrolase belonging to the “ α/β hydrolase fold” family characterized by a central β sheet core surrounded by a variable number of α helicals. The catalytic triad is formed by serine (S132), aspartic acid (D239) and histidine (H269) residues, in addition 3 cysteine residues appear to contribute to the regulation of MAGL functions (Figure 17).^{3,6}

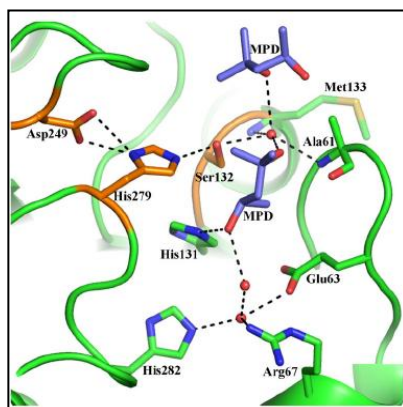


Figure 17

MAGL is involved in the inactivation of 2-AG, in particular it catalyses the hydrolysis of 2-AG to fatty acid and glycerol (Figure 18).^{3,6}

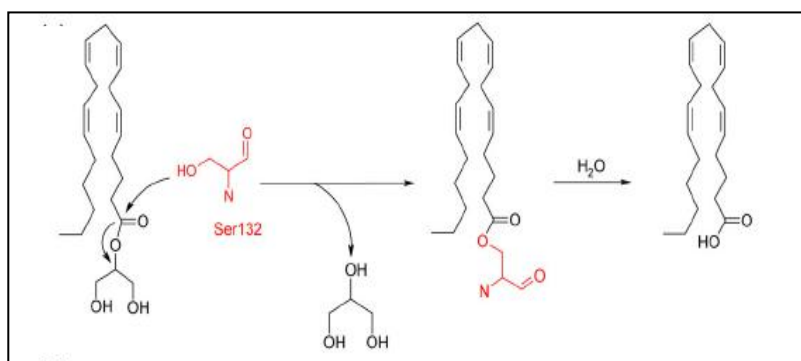


Figure 18

2.1 MAGL Inhibitors

There are different kinds of MAGL inhibitors, the major-ones are: NON-SPECIFIC SERINE HYDROLASE INHIBITORS, INHIBITORS INSPIRED BY THE ENDOGENOUS SUBSTRATE and *De novo* INHIBITORS.⁶

The main therapeutic applications of MAGL inhibitors are:

1. NEUROPROTECTION : they can protect neurons from hypoxic injury and they can protect from cerebral ischemia;⁶
2. FEEDING BEHAVIOUR: they can stimulate appetite, lipogenesis and fat accumulation;⁶
3. Treatment of CANCER: they can inhibit the proliferation of certain cancer cell lines;^{6,13}
4. Treatment of GLAUCOMA: they can regulate intraocular pressure;⁶
5. ANALGESIC EFFECTS.⁶

2.1.1 De novo Inhibitors

Some inhibitors of MAGL have been recently described whose structures do not resemble any endogenous cannabinoid: URB754, URB602 (Figure 19), SAR629 and JZL184 (Figure 20c).

- URB754 was reported to inhibit 2-AG degradation through a non competitive and irreversible mechanism;⁶
- URB602 showed a lower capacity to disrupt MAGL hydrolysing activity;⁶
- Other de novo INHIBITORS are: JZL184 a piperidine derivate and SAR629, a piperazine derivative, which exhibits interesting selectivity for MAGL over FAAH and showed a similar mechanism of inhibition. In particular, it is reported that SAR629 mechanism of inhibition mimics the pathway of 2-AG hydrolysis by MAGL by making a relatively stable carbamate adduct with the catalytic serine instead of the relatively labile ester adduct (Figure 20a and Figure 20b). MAGL–SAR629 co-structure permits the identification of pharmacophoric points (Figure 20c): the carbonyl oxygen of the urea function seems necessary to create the only polar interaction between the inhibitor and the Ser-132 of the protein. One of the fluorophenyl groups probably interacts with some hydrophobic residues and the role of the piperazine is to orient the other moieties toward pharmacophoric points, so it could probably be replaced by other moieties,^{3, 10}

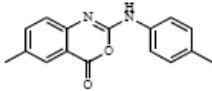
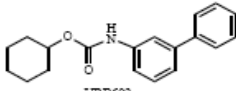
Compound	IC ₅₀ MAGL*
 URB754	200 ± 16 nM
 URB602	75 ± 7 μM 28 ± 4 μM ^c

Figure 19

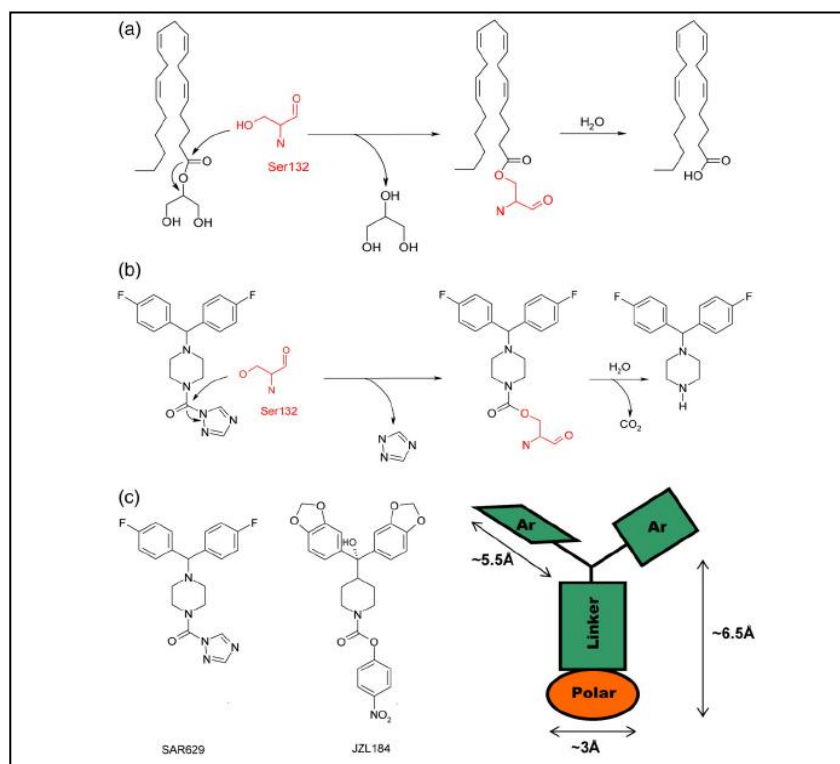


Figure 20

My thesis is on the design, synthesis and biological evaluation of quinolin-2-one derivatives and pyridin-2-one derivatives of general structure **A** and **B** respectively, as potential MAGL inhibitors. Compounds **A** and **B** could have the same interactions of compounds SAR-629 and JZL-184, with the active site of the enzyme, in fact for these compounds the carbonyl oxygen of the carbamate function could create the polar interactions with Ser 122 of the protein, the fluorophenyl group could interact with some hydrophobic residues and the quinoline or pyridine ring constitute the linker between the two pharmacophore groups of the molecule and could permit the adequate orientation of it into the active site of the enzyme.

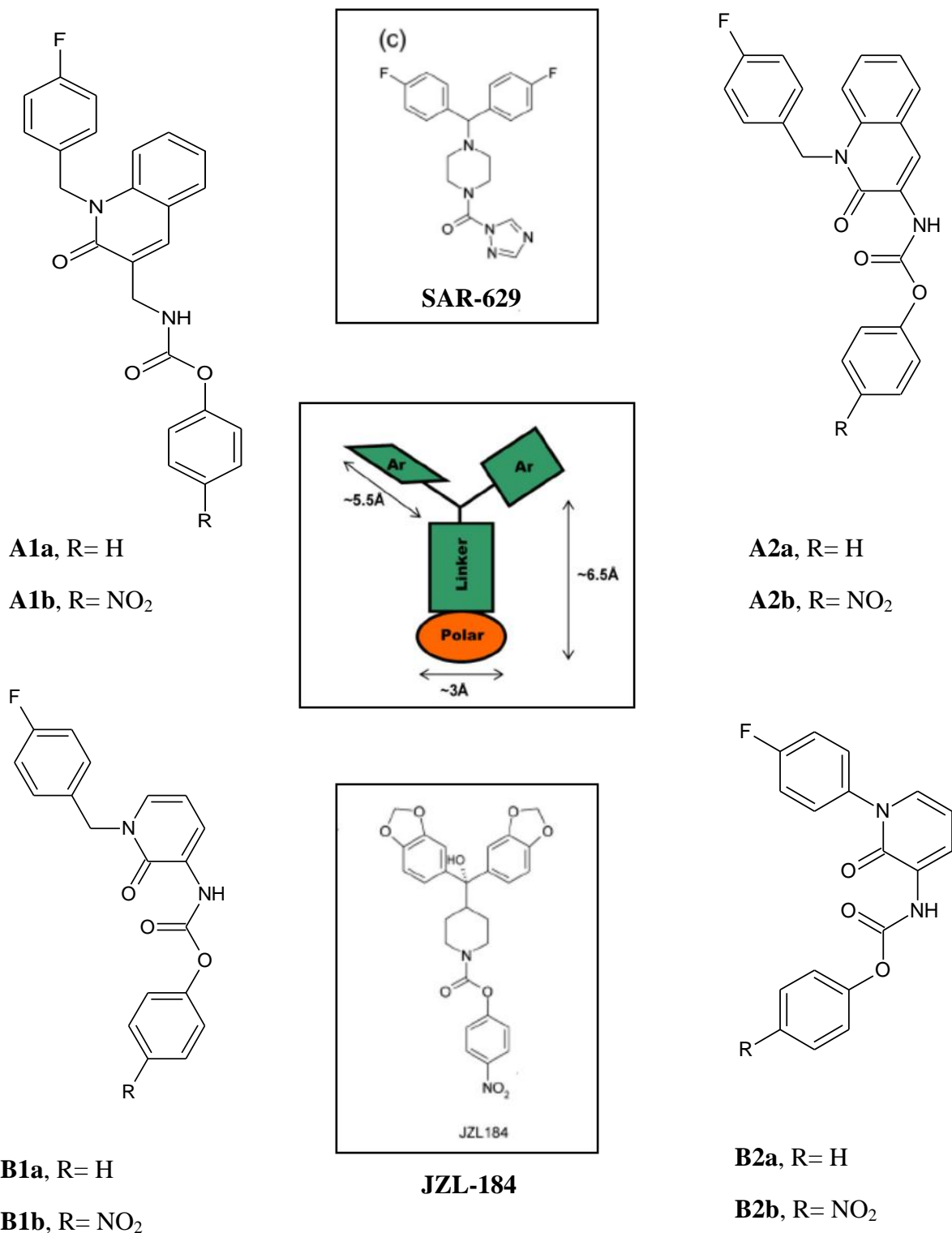


Figure 21

The synthesis of compounds **A1** were designed as describe in the Scheme 1. The 2-chloroquinoline-3-carboxaldehyde was refluxed with HCl 4N to afford the 2-oxo-quinoline-3-carboxaldehyde **1**. The treatment of derivative **1** in anhydrous DMF with cesium carbonate for 1 h

under stirring at room temperature and then with *p*-fluorobenzyl chloride at 50°C for 24 h gave the desired compound **2** purified by flash-chromatography using hexane/ethyl acetate 1:4. This compound was then allowed to react with hydroxylamine to afford the 3-hydroxyimino-quinolone **3** which for treatment with acetic anhydride under reflux for 2 h gave the 2-oxo-quinoline-3-carbonitrile **4**. The reduction of **4** with LiAlH₄ in various anhydrous solvents (Et₂O, CH₂Cl₂, THF) at room temperature or heated until reflux did not provide the desired aminomethyl derivative, in fact in the first case we recovered the starting product; instead in the second case, a mixture of difficult purification was obtained.

The compounds **A2** were obtained as reported in Scheme 2. The reaction between 3-bromo-quinoline and *m*-CPBA in CHCl₃ at room temperature for 20 hours afforded the N-oxide **5**. The reaction between compound **5** and benzoyl chloride, NaOH 1.5 M in CH₂Cl₂ at room temperature for 2 hours gave compound **6** as a crystalline pure solid. The bromo-quinoline **6** was treated with NaH in anhydrous DMF for 1 h and then with *p*-fluorobenzyl chloride to afford compound **7**. The desired compounds **A2a** and **A2b** were obtained by the palladium-catalyzed C–N coupling reaction between compound **7** and phenyl carbamate or *p*-nitrophenyl carbamate respectively, in 1,4-dioxane using palladium acetate as catalyst, Xantphos as ligand and Cs₂CO₃ as base at 100°C for 10 hours or using the microwave at 140°C for 38 minutes.

The synthesis of compounds **B** is depicted in the Scheme 3. The 2-hydroxy nicotinic acid was treated with NaH in anhydrous DMF for 2 h and then with *p*-fluorobenzyl chloride for 24 h at 50 °C to obtain a crude product which was treated with aqueous NaOH 10% under reflux for 4 hours to obtain the carboxylic acid **8**. The Curtius reaction between compound **8** and diphenylphosphorylazide, tBuOK in tBuOH afforded the corresponding BOC-derivative **9**, which was then hydrolyzed with HCl concentrate in order to obtain the amino-derivative **10**. The reaction between compound **10** and phenyl chloroformate, in presence of TEA in anhydrous CH₂Cl₂ at room temperature for 24 h gave the desired compound **B1a**. Instead, the reaction between the compound **10** and *p*-nitrophenyl chloroformate did not yield the desired compound **B1b**, probably because, at room temperature, the substrate is poorly reactive and at higher temperature the reagent goes through degradation.

The compounds **B2** were obtained as reported in Scheme 4, starting from methyl 2-oxo-2*H*-pyran-6-carboxylate. The Michael addition of 4-fluoroaniline to pyrane ester, followed by

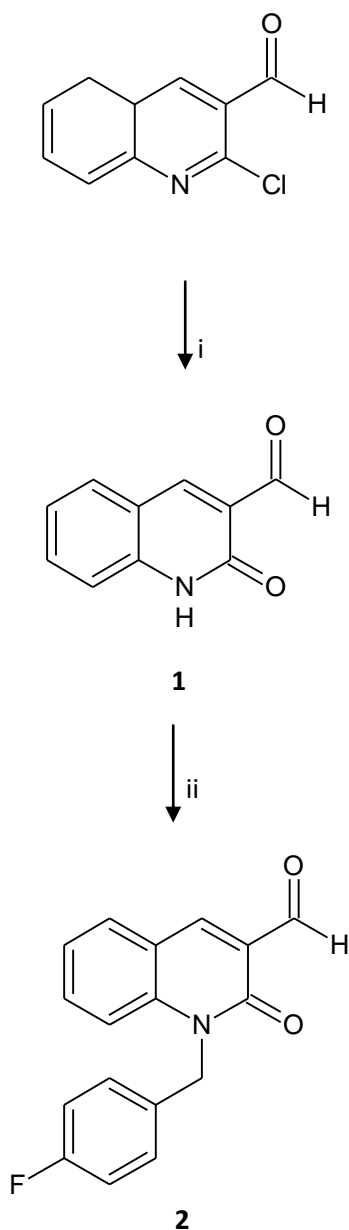
intramolecular cyclization of the Michael adduct provided *p*-fluorophenyl-2-pyridone ester **11**, which was hydrolyzed to afford *p*-fluorophenyl-2-pyridone acid **12**. The Curtius reaction, as reported before, between compound **12** with diphenyl-phosphorylazide, afforded the corresponding BOC-derivative **13**, which was hydrolyzed with HCl concentrate to give the amino-derivative **14**. The reaction between compound **14** and phenyl chloroformate, in presence of TEA in anhydrous CH₂Cl₂ at room temperature for 24 h gave the desired compound **B2a**. Also in this case the reaction between compound **14** and *p*-nitrophenyl chloroformate did not yield the desired compound **B2b**.

3. Equipment used in Synthesis

- Melting points were determined on a Kofler hot stage apparatus and are uncorrected.
- ¹H NMR spectra were recorded with a Bruker AC-200 spectrometer in δ unit from TMS as an internal standard.
- Analytical TLC was carried out on Merck 0.2 mm precoated silica-gel glass plates (60 F-254) and location of spots was detected by illumination with a UV lamp.

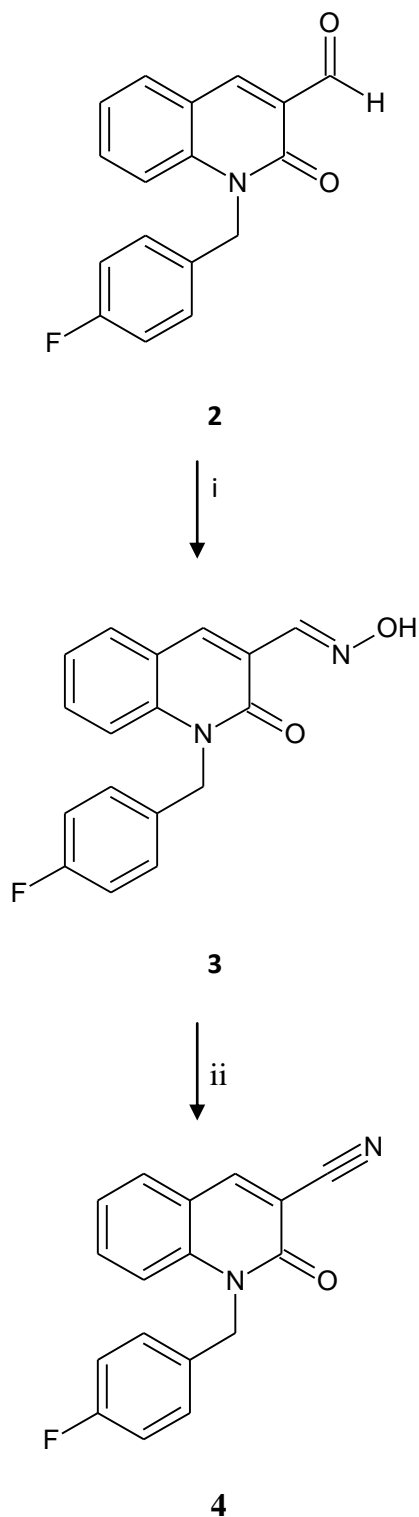
4. Scheme of Synthesis

4.1 Schema 1



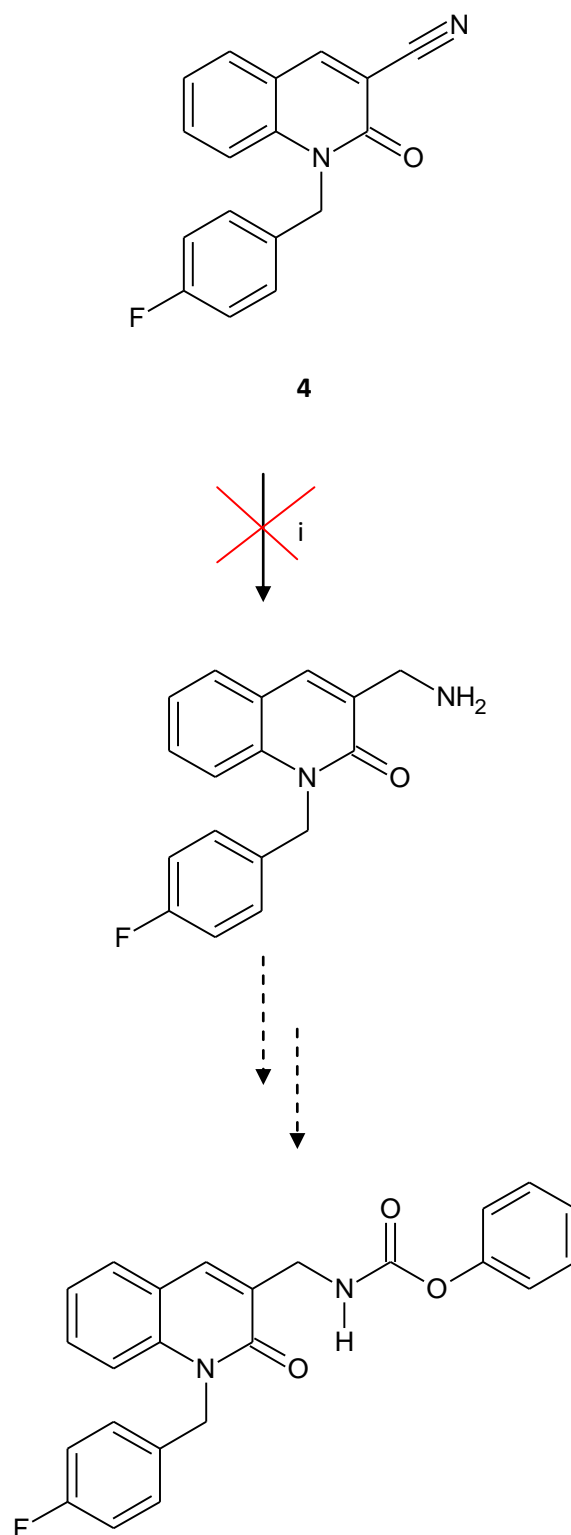
i: HCl 4N, 120°C, 2h. ii: Cs₂CO₃, anhydrous DMF, room T, 2h; 4-fluorobenzyl chloride, 50°C, 24h.

Schema 1 (continues)



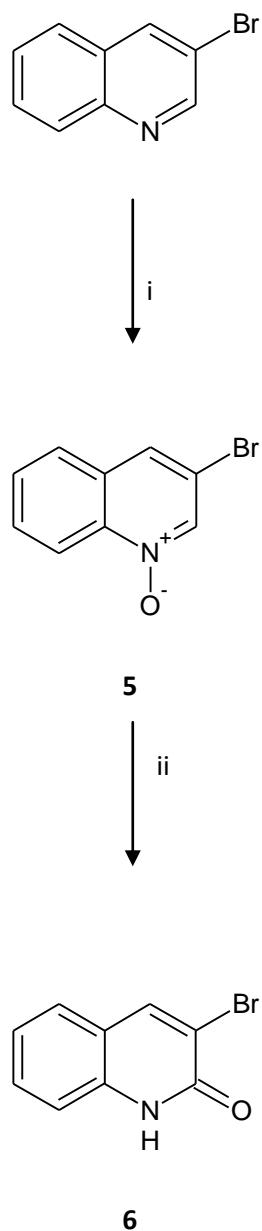
i: NH_2OH hydrochloride, NaOH 4N, 120°C , 2h. ii: acetic anhydride, 120°C , 4h.

Schema 1 (continues)



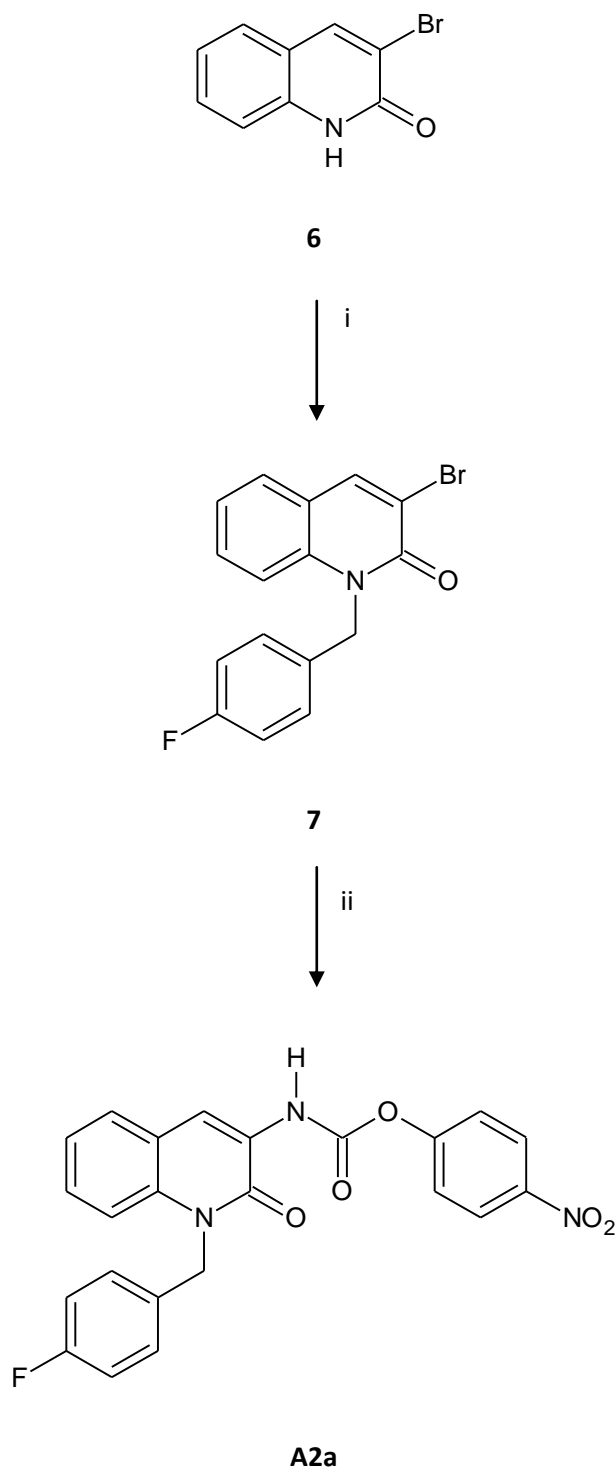
i: LiAlH_4 , anhydrous THF, 100°C , 4h.

4.2 Scheme 2



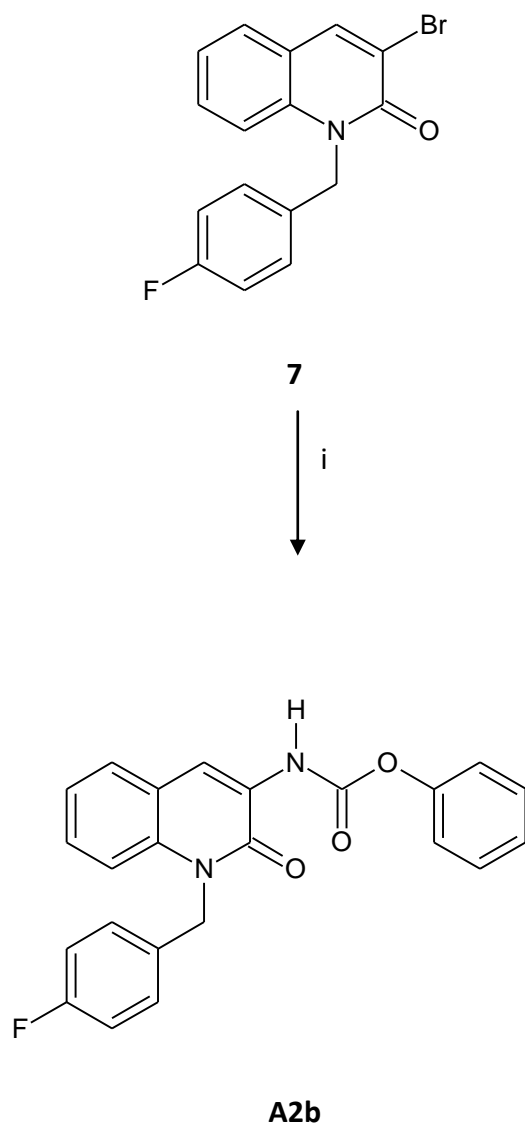
i: m-CPBA, CHCl_3 , 20h. ii: benzoyl chloride, $\text{NaOH}/\text{H}_2\text{O}$, CH_2Cl_2 , room temp., 2h.

Scheme 2 (continues)



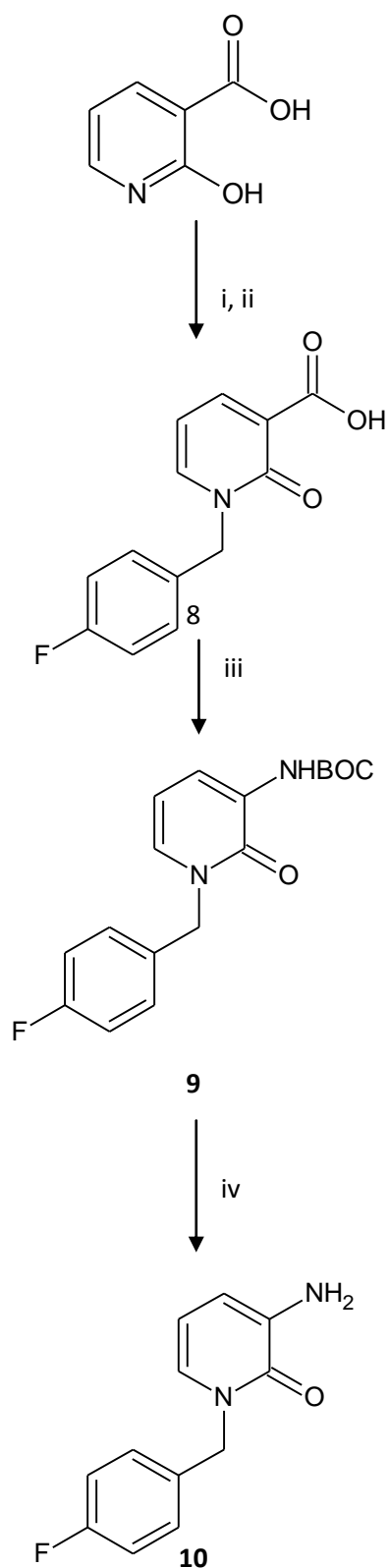
i: NaH, anhydrous DMF, 50°C, 2h; 4-fluorobenzyl chloride, room temp., 24h. ii: 4-nitrophenyl chloroformate, Pd(OAc)₂, Cs₂CO₃, Xantphos, dioxane, 100°C, 10h; or microwave conditions: 140°C, 125 Psi, 200 W, 38 min, stirring on, cooling on.

Scheme 2 (continues)



i: phenyl chloroformate, Pd(OAc)₂, Cs₂CO₃, Xantphos, dioxane, 100°C, 10h; or microwave conditions: 140°C, 125 Psi, 200 W, 38 min, stirring on, cooling on.

4.3 Schema 3

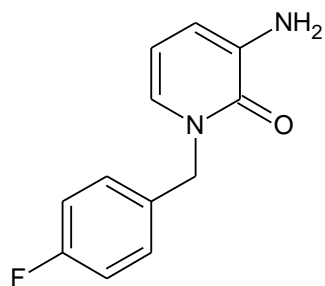


i: NaH , anhydrous DMF, room temp., 2h; 4-fluorobenzyl chloride, 50°C, 24h.

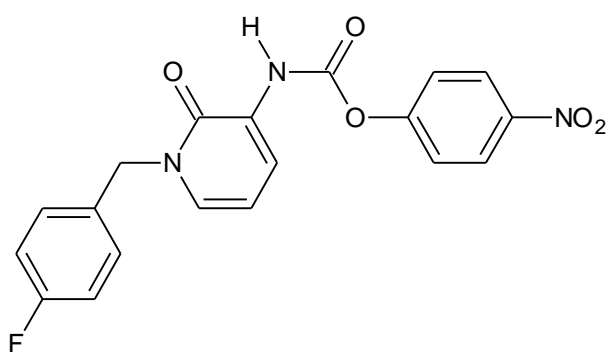
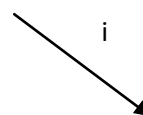
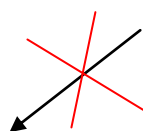
ii: NaOH 10%, 120°C, 24h. iii: Diphenyl phosphoryl azide, Tert-ButOK, Tert-ButOH, 100°C, 24h.

iv: HCl 6N, room temp., 4h.

Schema 3 (continues)



12

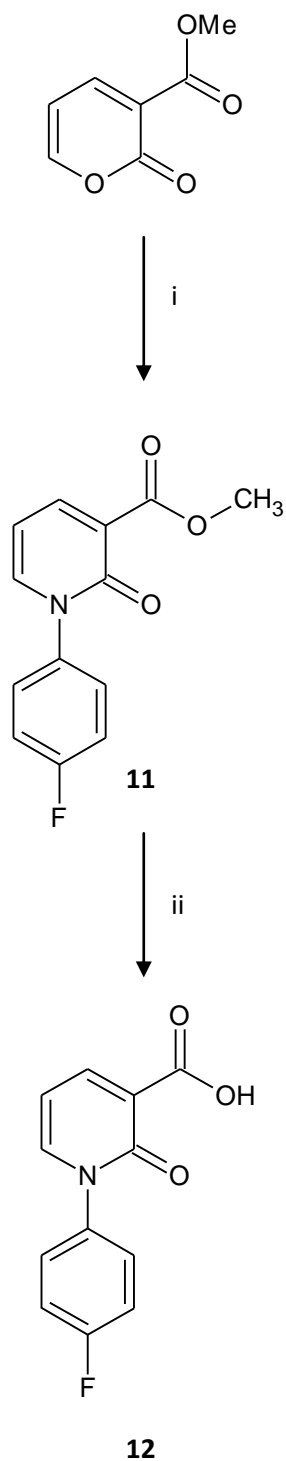


B1b

B1a

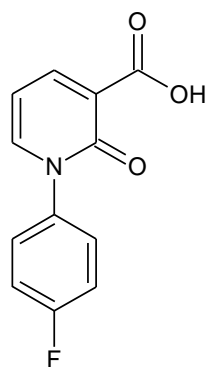
i: Phenyl chloroformate, TEA, anhydrous CH₂Cl₂, room temp., 4h.

4.4 Schema 4

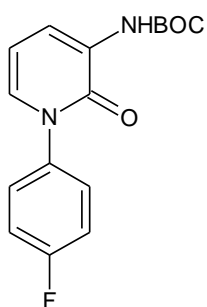


i: 4-fluoroaniline, anhydrous DMF, 0°C, 7h; DMAP, EDCI hydrochloride, room temp., overnight. ii: NaOH 10%, reflux, 4h.

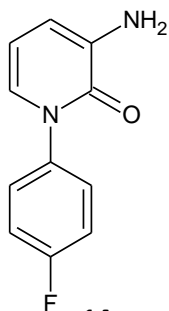
Schema 4 (continues)



12



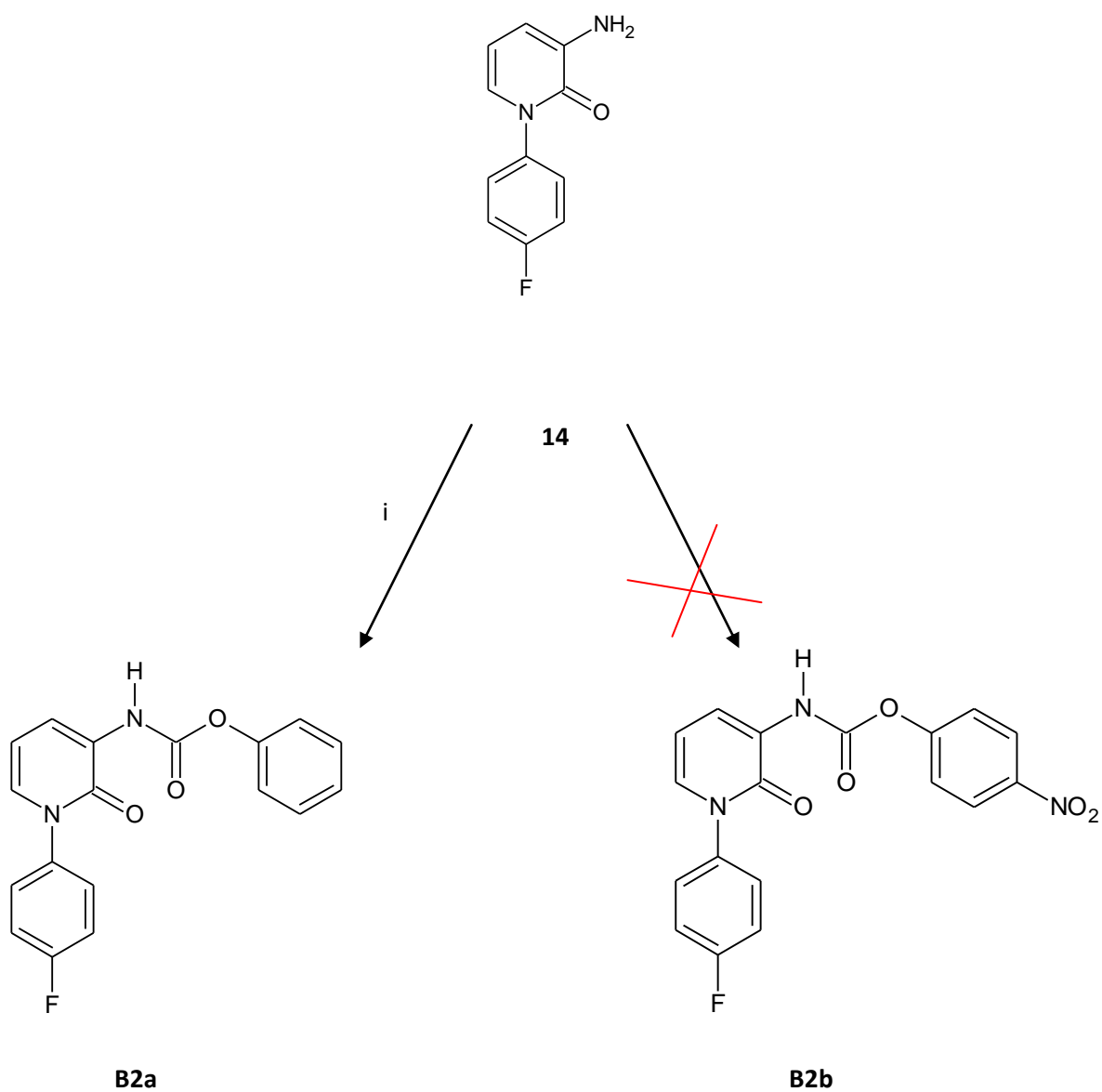
13



14

i: diphenyl phosphoryl azide, t-ButOK, t-ButOH, 100°C, 24h. ii: HCl 6N, room temp. , 4h.

Schema 4 (continues)



i: Phenyl Chloroformate, TEA, anhydrous CH_2Cl_2 , room temp., 4h .

5. Experimental Part

5.1 2-oxo-1,2-dihydro quinoline-3-carboxaldehyde (1)

An amount of 0,500 g (2,58 mmol) of 2-Chloroquinoline-3-carboxaldehyde was heated under reflux in 18,5 ml of HCl 4N for one hour. After cooling the precipitate was washed with water and collected by filtration. The precipitate obtained was dried under vacuum for 24 Hours.

Yield: 92%

Mp: 252-255 °C

¹H-NMR: (DMSO) δ 12,5 (s, 1H, NH); 10,24 (s,1H, CHO); 8,51 (s,1H, H₄); 7,92 (d,1H, H₈); 7,37 (t,1H, H₇); 7,29 (d, 1H, H₆); 7,25 (t, 1H, H₅).

5.2 1-(4-fluorobenzyl)-2-oxo-1,2-dihydro quinoline-3-carboxaldehyde (2)

An amount of 1,50 g (4,62 mmol) of Cs_2CO_3 was added to a solution of 0,400 g (2,31 mmol) of **1** in 20 ml of anhydrous DMF and the mixture was stirred at room temperature for two hours. After that 0,42 ml of 4-fluorobenzyl chloride (3,47 mmol) was added dropwise and the mixture was stirred at 50°C for 24 hours. Furthermore the solution was concentrated under vacuum and the crude product obtained was purified by flash-chromatography (eluent: 4 ethyl-acetate/ 1 hexane) in order to obtain compound **3** as a crystalline solid.

Yield: 75%

Mp: 267-270°C

¹H-NMR: (DMSO) δ 10,33 (s, 1H, CHO); 8,61 (s, 1H, H₄); 8,05 (d, 1H, H₅); 7,69 (d, 1H, phenyl group); 7,48 (d, 1H, phenyl group); 7,34 (d, 1H, H₈); 7,15 (m, 2H, H₆;H₇); 5,57 (s, 1H, CH₂)

5.3 1-(4-fluorobenzyl)-3-[(hydroxyimino)methyl]quinolin-2(1H)-one (3)

An amount of 5,00 ml of NaOH 4M was added to a solution of 0,250 g (0,89 mmol) of **2** in 30 ml of ethanol, after that 0,300 g (9,09 mmol) of hydroxylamine hydrochloride was added and the mixture was heated under reflux. After 2 hours the solution was cooled into ice bath and acidified with HCl 37% (pH= 4) to obtain a precipitate which was collected by filtration and dried under vacuum.

Yield: 75%

Mp : 265-267°C

¹H-NMR: (DMSO) δ 11,57 (s, 1H, OH oxime); 8,38 (s, 1H, CH oxime); 8,30 (s, 1H, H₄); 7,83 (d, 1H, H₅); 7,58 (d, 2H, phenyl group); 7,50 (d, 1H, H₈); 7,48 (m, 2H, H₆; H₇); 5,56 (s, 2H, CH₂).

5.4 1-(4-fluorobenzyl)-2-oxo-1,2-dihydroquinoline-3-carbonitrile (**4**)

An amount of 0,170 g (0,57 mmol) of **3** was added to a solution of 10 ml of acetic anhydride and the mixture was heated under reflux for 2 hours. After that the mixture was cooled into ice bath and alkalized with NaOH until pH=10-11. The precipitate obtained was filtered and dried under reduced pressure. The dry precipitate was purified by flash-chromatography (eluent: 5 hexane/ 3 ethyl acetate) in order to obtain compound **4** as a crystalline solid.

Yield: 63%

Mp: 232-235°C

¹H-NMR: (DMSO) δ 8,91 (s, 1H, H₄); 7,87 (d,1H, H₅); 7,70 (d, 2H, phenyl group); 7,45 (d, 2H, phenyl group); 7,33 (m, 3H, H₆, H₇, H₈); 5,54 (s, 1H, CH₂).

5.5 3-bromoquinoline 1-oxide (5)

An amount of 0,508 g (2,95 mmol) of m-CPBA was added to a solution of 0,600 g (2,88 mmol) of 3-bromo-quinoline in 10 ml of CHCl₃. The mixture was stirred at room temperature for 20 hours. Then the mixture was diluted with NaHCO₃ and NaOH and extracted with CHCl₃, the organic layer was dried with MgSO₄ and concentrated under reduced pressure to obtain a crude product. The crude was treated with petroleum ether and the precipitate obtained was collected by filtration in order to obtain **5**.

Yield: 58%

Mp: 191-196°C

¹H-NMR: (DMSO) 8,70-8,63 (m, 2H, H₄;H₂); 7,90-7,67 (m, 4H, H₅, H₆, H₇, H₈);

5.6 3-bromoquinolin-2(1H)-one (6)

An amount of 4 ml of NaOH 1,5N (3,00 mmol) and 0,20 ml (1,68 mmol) of benzoyl chloride was added to a solution of 0,300 g (1,40 mmol) of **5** in 5 ml of CH₂Cl₂. After that the mixture was stirred at 0°C for 2 hours into ice bath, the precipitate obtained was collected by filtration to obtain **6**.

Yield: 80%

Mp: 215-217°C

¹H-NMR: (DMSO) δ 11,47 (s, 1H, NH); 8,26 (s, 1H, H₄); 7,56 (d, 1H, H₅); 7,43 (d, 1H, H₈); 7,28 (m, 2H, H₆, H₇).

5.7 3-bromo-1-(4-fluorobenzyl)quinolin-2(1H)-one (7)

An amount of 0,083 g (3,47 mmol) of NaH was added to a solution of 0,500 g (2,89 mmol) of **6** in 20 ml of anhydrous DMF and the mixture was stirred at room temperature for two hours. After that 38 ml of 4-fluorobenzyl chloride (3,47 mmol) was added dropwise and the mixture was stirred at 50°C for 24 hours. Furthermore the solution was concentrated under vacuum, the crude product was treated with water and the precipitate obtained was purified by flash-chromatography (eluent: 4 ethyl-acetate/ 1 hexane) in order to obtain compound **7** as a crystalline solid.

Yield: 57%

Mp: 224-227°C

¹H-NMR: (DMSO) δ 8,21 (s, 1H, H₄); 7,50 (m, 2H, H₅, H₈) 7,27 (m, 4H, phenyl group); 7,05 (m, 2H, H₆, H₇); 5,58 (s, 2H, CH₂).

5.8 4-nitrophenyl [1-(4-fluorobenzyl)-2-oxo-1,2-dihydroquinolin-3-yl]carbamate (A2a)

An amount of 0,124 g (0,37 mmol) of **7** was added, under nitrogen flow, to a suspension of 0,005 g (0,03 mmol) of Pd(AcO)₂, 0,010 g (0,02 mmol) of Xantphos, 0,150 g (0,82 mmol) of 4-nitrophenyl carbamate and 0,294 g (0,90 mmol) of Cs₂CO₃ in 7 ml of dioxane. The mixture was heated at 100°C for 10 hours, after that it was cooled, filtered and concentrated under reduced pressure. The crude product obtained was purified by flash-chromatography (eluent:CH₂Cl₂) in order to obtain compound **A2a** as a light brown solid.

The same reaction was also done using the microwave with the following conditions: T=140°C, t=37min 30sec, P=5 Bar, stirring on, cooling on. The mixture was then cooled, filtered and concentrated under reduced pressure. The crude product obtained was purified by flash-chromatography (eluent:CH₂Cl₂) in order to obtain compound **A2a** as a light brown solid.

Yield: 35%

Mp: 238-241°C

¹H-NMR: (DMSO) δ 8,32 (s, 1H, NH carbamate); 7,85 (s, 1H, H₄); 7,81 (s, 1H, H₈); from 7,57 to 7,45 (m, 4H, phenyl group); from 7,38 to 7,13 (m, 7H, phenyl group; H₅; H₆; H₇); 5,61 (s, 2H, CH₂).

5.9 Phenyl [1-(4-fluorobenzyl)-2-oxo-1,2-dihydroquinolin-3-yl]carbamate (**A2b**)

An amount of 0,124 g (0,37 mmol) of **7** was added, under nitrogen flow, to a suspension of 0,005 g (0,03 mmol) of Pd(AcO)₂, 0,010 g (0,02 mmol) of Xantphos, 0,112 g (0,82 mmol) of phenyl carbamate and 0,294 g (0,90 mmol) of Cs₂CO₃ in 7ml of dioxane. The mixture was heated at 100°C for 10 hours, after that it was cooled, filtered and concentrated under reduced pressure. The crude product obtained was purified by flash-chromatography (eluent:CH₂Cl₂) in order to obtain compound **A2b** as a light brown solid.

The same reaction was also done using the microwave with the following conditions: T=140°C, t=37min 30sec, P=5Bar, stirring on, cooling on. The mixture was then cooled, filtered and concentrated under reduced pressure. The crude product obtained was purified by flash-chromatography (eluent:CH₂Cl₂) in order to obtain compound **A2b** as a light brown solid.

Yield: 33%

Mp: 231-233°C

¹H-NMR: (DMSO) δ 8,31 (s, 1H, NH carbamate); 7,83 (s, 1H, H₄); 7,81 (s, 1H, H₈); from 7,57 to 7,40 (m, 4H, phenyl group); from 7,33 to 7,10 (m, 7H, phenyl group; H₅; H₆; H₇); 5,51 (s, 2H, CH₂).

5.10 4-fluorobenzyl 1-(4-fluorobenzyl)-2-oxo-1,2-dihydropyridine-3-carboxylate (**8**)

An amount of 0,650 g (12,9 mmol) of NaH was added to a solution of 1,50 g (10,79 mmol) of 2-hydroxy nicotinic acid in 20 ml of anhydrous DMF and the mixture was stirred at room temperature for two hours. After that 1,50 ml (12,9 mmol) of 4-fluorobenzyl chloride was added dropwise and the mixture was stirred at 50°C for 24 hours. Furthermore the solution was concentrated under vacuum and the crude product obtained was washed with water and collected by filtration. The crude mixture was added to a solution of NaOH 10% and heated under reflux for 4 hours. Then the solution was cooled into ice bath and acidified until acid pH. The precipitate obtained was collected by filtration in order to obtain compound **8** as a crystalline solid.

Yield: 75%

Mp: 221-224°C

¹H-NMR: (DMSO) δ 14,40 (s, 1H, COOH); 8,40 (m, 2H, H₄, H₆); 7,41 (d, 2H, phenyl group); 7,18 (d, 2H, phenyl group); 6,48 (t, 1H, H₅); 5,28 (s, 2H, CH₂).

5.11 Tert-butyl [1-(4-fluorobenzyl)-2-oxo-1,2-dihydropyridin-3-yl]carbamate (**9**)

An amount of 1,05 ml (4,85 mmol) of diphenyl phosphoryl azide was added to a solution of 1,00 g (4,05 mmol) of **8** and 0,590g (4,85 mmol) of Tert-ButOK in 25 ml of Tert-ButOH. The mixture was heated under reflux for 24 hours, after that the mixture was diluted with CH₂Cl₂, washed with water and dried with MgSO₄. The organic layer was concentrated under reduced pressure in order to give a crude product as a brown oil. The crude product was purified by flash-chromatography (eluent: 3 hexane/1 ethyl acetate) in order to obtain **9** as a crystalline solid.

Yield: 25%

Mp: 230-233°C

¹H-NMR: (DMSO) δ 8,6 (s, 1H, NH carbamate); 7,81 (d, 1H, H₄); 7,55 (d, 1H, H₆); 7,37 (m, 2H, phenyl group); 7,16 (m, 2H, phenyl group); 5,15 (s, 2H, CH₂); 1,46 (s, 9H, t-butyl).

5.12 3-amino-1-(4-fluorobenzyl)pyridin-2(1H)-one (**10**)

An amount of 0,300 g (0,94 mmol) of **9** was added to 16ml of HCl 6N and the mixture was stirred at room temperature for 4 hours. After that the solution was neutralized with NaHCO₃ and the product was extracted with CH₂Cl₂. The organic layer was dried with anhydrous MgSO₄ and evaporated under reduced pressure to give **10** as a brown oil.

Yield: 95%

¹H-NMR: (DMSO) δ 7,32 (m, 2H, phenyl group); 7,29 (m, 2H, phenyl group); 7,17 (d, 1H, H₄); 6,42 (d, 1H, H₆); 5,11 (s, 1H, NH₂); 5,05 (s, 2H, CH₂).

5.13 Phenyl [1-(4-fluorobenzyl)-2-oxo-1,2-dihydropyridin-3-yl]carbamate (B1a)

An amount of 0,44 ml (2,73mmol) of phenyl chloroformate was added dropwise to a solution of 0,300 g(1,05mmol) of **10** and 0,38 ml of TEA (2,73 mmol) in 10 ml of anhydrous CH₂Cl₂. After that the mixture was stirred at room temperature for 24 hours, it was evaporated under vacuum and the crude product obtained washed with water, treated with diethyl ether and collected by filtration.

Yield: 65%

Mp: 135-138°C

¹H-NMR: (DMSO) δ 8,95 (s, 1H, H carbamate); 7,83 (d, 1H, H₄); 7,80 (d, 1H, H₆); 7,61-7,17 (m, 8H, phenyl group); 6,75 (m, 1H, phenyl group); 6,32 (t, 1H, H₅); 5,164 (s, 2H, CH₂).

5.14 Methyl 1-(4-fluorophenyl)-2-oxo-1,2-dihydropyridine-3-carboxylate (11)

An amount of 0,37 ml (3,90 mmol) of 4-Fluoroaniline was added to a solution of 1,00 g (3,25 mmol) of methyl 2-oxo-2*H*-pyran-6-carboxylate in 10 ml of anhydrous DMF. The solution was stirred at 0°C for 7 hours into ice bath, after that was added an amount of 0,100g (0,81 mmol) of DMAP and 0,810 g (4,22 mmol) of EDCI hydrochloride. The mixture was stirred overnight at room temperature, then the solution was concentrated under reduced pressure to obtain a crude product. The crude was washed with water and the organic layer was extracted with ethyl acetate. The organic layer was dried with MgSO₄ and was concentrated under reduced pressure to obtain a second crude product, which was purified by flash-chromatography (eluent: 3ethyl acetate/1hexane) in order to obtain **11** as a crystalline solid.

Yield: 57%

Mp: 219-221°C

¹H-NMR: (DMSO) δ 8,10 (dd, 1H, H₄); 7,92 (dd, 1H, H₆); 7,45 (m, 2H, phenyl group); 7,33 (m, 2H, phenyl group); 6,37 (t, 1H, H₅); 3,71 (s, 3H, OCH₃).

5.15 1-(4-fluorophenyl)-2-oxo-1,2-dihydropyridine-3-carboxylic acid (12)

An amount of 0,450 g (1,82 mmol) of **11** was added to a solution of NaOH 10%, and the mixture was heated under reflux for 4 hours, the mixture was acidified into ice bath and the precipitate obtained was collected by filtration.

Yield: 80%

Mp: 225-228°C

¹H-NMR: (DMSO) δ 14,23 (s, 1H, COOH); 8,47 (dd, 1H, H₄); 8,20 (dd, 1H, H₆); 7,51 (m, 2H, phenyl group); 7,41 (m, 2H, phenyl group); 6,77 (t, 1H, H₅).

5.16 Tert-butyl [1-(4-fluorophenyl)-2-oxo-1,2-dihydropyridin-3-yl]carbamate (**13**)

An amount of 0,40 ml (1,8 mmol) of diphenyl phosphoryl azide was added to a solution of 0,350 g (1,50 mmol) of **12** and 0,133 g (1,8 mmol) of Tert-ButOK in 25 ml of Tert-ButOH. The mixture was heated under reflux for 24h. After that the solution was diluted with CH₂Cl₂, washed with water and the organic layer was dried with MgSO₄, concentrated under reduced pressure in order to obtain compound **13** as a crystalline solid.

Yield: 43%

Mp: 229-231°C

¹H-NMR: (DMSO) δ 8,76 (s, 1H, NH carbamate); 7,81 (dd, 1H, H₄); 7,55 (dd, 1H, H₆); 7,37- 6,93 (m, 4H, phenyl group); 6,33 (t, 1H, H₅); 1,43 (s, 9H, t-Butyl).

5.17 3-amino-1-(4-fluorophenyl)pyridin-2(1H)-one (**14**)

An amount of 0,150 g (0,49mmol) of **13** was added to a solution of HCl 6N and the mixture was stirred at room temperature for 4 hours. After that the solution was neutralized with NaHCO₃ and the product was extracted with CH₂Cl₂. The organic layer was dried with anhydrous MgSO₄ and evaporated under reduced pressure in order to obtain **14** as a brown oil.

Yield: 90%

¹H-NMR: (DMSO) δ 7,41 (m, 2H, phenyl group); 7,36 (m, 2H, phenyl group); 6,75 (dd, 1H, H₄); 6,58 (dd, 1H, H₆); 6,15 (t, 1H, H₅); 4,31(s, 1H, NH₂).

5.18 Phenyl [1-(4-fluorophenyl)-2-oxo-1,2-dihydropyridin-3-yl]carbamate (B2a)

An amount of 0,10 ml (0,61 mmol) of phenyl chloroformate was added dropwise to a solution of 0,050 g (0,25 mmol) of **14** and 0,085ml of TEA (6,21 mmol) in 10 ml of anhydrous CH₂Cl₂. After that the mixture was stirred for 24 hours at room temperature, it was evaporated and the crude product obtained was washed with water, treated with diethyl ether and collected by filtration to give **B2a**.

Yield: 62%

Mp: 145-148°C

¹H-NMR: (DMSO) δ 8,99 (s, 1H, H carbamate); 8,18 (dd, 1H, H₄); 7,90 (dd, 1H, H₆); from 7,49 to 7,17 (m, 9H, phenyl group); 6,38 (t, 1H, H₅).

6. References

1. Cristiana Moliterni, V.M. Luigi Cattivelli, P. Ranalli and Giuseppe Mandolino. 2005. The sexual differentiation of *Cannabis sativa* L.: A morphological and molecular study. *Euphytica* 140 (1-2): 95-106. Retrieved on 25 Feb 2007.,
2. K. H. Ratio et al. *Current medicinal chemistry* 2005, 12, (1217/1237).
3. Séverine Vandevoorde; Overview of the Chemical Families of Fatty Acid Amide Hydrolase and Monoacylglycerol Lipase Inhibitors; *Current Topics in Medicinal Chemistry*, 2008, 8, 247-267.
4. Sugiura, T., Kondo, S., Sukagawa, A., Nakane, S., Shinoda, A., Itoh, K. et al. (1995). 2-Arachidonoylglycerol: a possible endogenous cannabinoid receptor ligand in brain. *Biochem. Biophys. Res. Commun.* 215, 89–97.
5. Piomelli, D., Giuffrida, A., Calignano, A. & Rodriguezde, F. F. (2000). The endocannabinoid system as a target for therapeutic drugs. *Trends Pharmacol. Sci.* 21, 218–224.
6. Alma Viso, José A. Cisneros and Silvia Ortega-Gutiérrez; The Medicinal Chemistry of Agents Targeting Monoacylglycerol Lipase; *Current Topics in Medicinal Chemistry*, 2008, 8, 231-246.
7. Aron H. Lichtman, Jacqueline L. Blankman, and Benjamin F. Cravatt, Endocannabinoid Overload, *Mol Pharmacol* 78:993–995, 2010.
8. Heikki Kennen, Mikko J. Myllymki, Anna Minkkil, Antti O. Kataja, Susanna M. Saario, Tapio Nevalainen, Ari M. P. Koskinen, and Antti Poso; 3-Heterocycle-Phenyl N-Alkylcarbamates as FAAH inhibitors: Design, Synthesis and 3D-QSAR Studies; *ChemMedChem* 2010, 5, 213 – 231.
9. *ChemBioChem* 2010, 11, 218-227.
10. T Bertrand et al. *J. Mol. Biol.* 2010, 396, 663-673.
11. Tamada, T., Kinoshita, T., Kurihara, K., Adachi, M., Ohhara, T., Imai, K. et al. (2009). Combined highresolution neutron and X-ray analysis of inhibited elastase confirms the active-site oxyanion hole but rules against a low-barrier hydrogen bond. *J. Am. Chem. Soc.* 131, 11033–11040.
12. *Chem. Soc.* 131, 11033–11040.
13. Jonathan Z. Long, Xin Jin, Alexander Adibekian, Weiwei Li, and Benjamin F. Cravatt; Characterization of Tunable Piperidine and Piperazine Carbamates as Inhibitors of Endocannabinoid Hydrolases; *Journal of Medicinal Chemistry*, XXXX, Vol. XXX, No. XX.

14. Ligresti, A., Bisogno, T., Matias, I., De Petrocellis, L., Cascio, M. G., Cosenza, V. et al. (2003). Possible endocannabinoid control of colorectal cancer growth. *Gastroenterology*, 125, 677–687.
15. T. Bisogno et al. / *Biochimica et Biophysica Acta* XX (2006) XXX-XXX.
16. Jonathan Z. Long, Daniel K. Nomura, and Benjamin F. Cravatt. Characterization of Monoacylglycerol Lipase Inhibition Reveals Differences in Central and Peripheral Endocannabinoid Metabolism. *Chemistry & Biology* 16, 744–753, July 31, 2009.